M/L_B AND COLOR EVOLUTION FOR A DEEP SAMPLE OF $M^\star$ CLUSTER GALAXIES AT $z \sim 1$: THE FORMATION EPOCH AND THE TILT OF THE FUNDAMENTAL PLANE[*,†,‡]

B. P. HOLDEN[1], A. VAN DER WEL[2], D. D. KELSON[3], M. FRANX[4], AND G. D. ILLINGWORTH[1]

[1] UCO/Lick Observatories, University of California, Santa Cruz, CA 95065, USA; holden@ucolick.org, gdi@ucolick.org
[2] Max-Planck Institute for Astronomy, Königstuhl 17, D-69117, Heidelberg, Germany; vdwel@mpia.de
[3] Observatories of the Carnegie Institution of Washington, Pasadena, CA 91101, USA; kelson@obs.carnegiescience.edu
[4] Sterrewacht Leiden, P.O. Box 9513, 2300 RA, Leiden, The Netherlands; franx@strw.leidenuniv.nl

ABSTRACT

We have measured velocity dispersions (σ) for a sample of 36 galaxies with $J < 21.2$ or $M_r < -20.6$ mag in MS 1054-03, a massive cluster of galaxies at $z = 0.83$. Our data are of uniformly high quality down to our selection limit, our 16 hr exposures typically yielding errors of only $\delta(\sigma) \sim 10\%$ for L^* and fainter galaxies. By combining our measurements with data from the literature, we have 53 cluster galaxies with measured dispersions, and HST/ACS-derived sizes, colors and surface brightness. This sample is complete for the typical $L^\star$ galaxy at $z \sim 1$, unlike most previous $z \sim 1$ cluster samples which are complete only for the massive cluster members ($>10^{11} M_\odot$). We find no evidence for a change in the tilt of the fundamental plane (FP). Nor do we find evidence for evolution in the slope of the color–σ relation and M/L_B–σ relations; measuring evolution at a fixed σ should minimize the impact of structural evolution found in other work. The M/L_B at fixed σ evolves by $\Delta \log_{10} M/L_B = -0.50 \pm 0.03$ between $z = 0.83$ and $z = 0.02$ or $d \log_{10} M/L_B = -0.60 \pm 0.04 \, dz$, and we find $\Delta(U - V)_z = -0.24 \pm 0.02$ mag at fixed σ in the rest frame, matching the expected evolution in M/L_B within 2.25 standard deviations. The implied formation redshift from both the color and M/L_B evolution is $z_\star = 2.0 \pm 0.2 \pm 0.3$(sys), during the epoch in which the cosmic star formation activity peaked, with the systematic uncertainty showing the dependence of $z_\star$ on the assumptions we make about the stellar populations. The lack of evolution in either the tilt of the FP or in the M/L–σ and color–σ relations imply that the formation epoch depends weakly on mass, ranging from $z_\star = 2.3^{+1.3}_{-0.3}$ at $\sigma = 300$ km s^{-1} to $z_\star = 1.7^{+0.3}_{-0.2}$ at $\sigma = 160$ km s^{-1} and implies that the initial mass function similarly varies slowly with galaxy mass.

Key words: galaxies: clusters: general – galaxies: clusters: individual (EMSS 1054.4-0321) – galaxies: elliptical and lenticular, cD – galaxies: evolution – galaxies: fundamental parameters – galaxies: photometry

Online-only material: color figures

1. INTRODUCTION

The evolution of the mass-to-light ratio (M/L) of early-type galaxies can be measured by combining the velocity dispersion (σ), the effective radius (r_e), the average surface brightness within the effective radius ($\langle I_e \rangle$), with which we can measure $M/L \propto \sigma^2/(r_e \langle I_e \rangle)$ and how it depends on mass, $M \propto r_e \sigma^2$. Typically, these three variables are combined into an empirical relation such as $r_e \propto \sigma^{1.20} \langle I_e \rangle^{-0.83}$ (Jørgensen et al. 1996, hereafter JFK96), known as the fundamental plane (FP; Faber et al. 1987; Djorgovski & Davis 1987).

The absolute M/L value and the how fast the M/L evolves with time can be used as a technique for measuring the age of stellar population (Tinsley 1972). The younger the population, the more luminous the stars, and so it will have lower M/L values and the M/L will evolve faster. Massive cluster galaxies, those galaxies with $M > 10^{11} M_\odot$ where $M \propto \sigma^2 r_e$, out to

$z \geqslant 1$ appear to evolve as $\Delta \ln M/L_B \simeq z$ (van Dokkum & Franx 1996, 2001; Kelson et al. 1997, 2000c; van Dokkum & Stanford 2003; Wuyts et al. 2004; Holden et al. 2005b; van Dokkum & van der Marel 2007). This rate of evolution is also seen in some field samples, though there is a larger scatter for the latter (van Dokkum et al. 2001; Gebhardt et al. 2003; van Dokkum & Ellis 2003; van de Ven et al. 2003; van der Wel et al. 2004, 2005; Treu et al. 2005a, 2005b). This rate of evolution implies an epoch of formation for the stars in early-type galaxies of $z_\star \simeq 2$, assuming a passively evolving simple stellar population with a standard Salpeter-like initial mass function (IMF). This redshift is near the peak of star formation (e.g., Madau et al. 1998; Steidel et al. 1999; Dickinson et al. 2003; Rudnick et al. 2003). Thus, the majority of stars in massive early-type galaxies formed around the time that the average star in the universe was formed.

The FP results of Treu et al. (2005b, hereafter T05) find that for galaxies with masses of $<10^{11} M_\odot$, the M/L values are lower and evolve more rapidly than those for higher mass galaxies. This implies a typical luminosity-weighted age of the stellar populations corresponding to a redshift between $z_\star = 1$ and $z_\star = 2$. van Dokkum & van der Marel (2007, hereafter vv07) confirmed that at redshifts of $z \simeq 1$, the FP of cluster galaxies shows a different distribution of M/L values than at $z \simeq 0$ with some lower mass galaxies ($<10^{11} M_\odot$) having low M/L and potentially more recent epochs of formation than the higher mass galaxies. Jørgensen et al. (2006, 2007) found a correspondingly steeper tilt to the FP for cluster galaxies in

RX J0152-13, indicating that cluster galaxies show similar behavior to field galaxies, though with a smaller magnitude effect. Similar results are clearly seen in Saglia et al. (2010) which jointly studies a field and cluster sample with a uniform selection. The observed increase in the tilt of the FP was interpreted as a younger average stellar population age. However, for a sample limited in L, only those galaxies with a low M/L will appear at low masses. van der Wel et al. (2005, vdW05) showed that it is difficult to distinguish between evolution in the tilt and in the scatter of the FP. This is the direct result of the selection by optical magnitude in their sample. They conclude that the $z \sim 1$ FP is likely to be different from the present-day FP, but that the form (tilt or scatter) of the evolution is not constrained besides the evolution in the zero point at high mass.

Younger stellar populations will not only have a lower M/L, but also have bluer colors. As we look to higher redshift stellar populations where the slope of the FP appears to tilt, we should see a corresponding trend of bluer galaxies at lower mass, or a change in both the slope of the color–magnitude and color–mass relations, with the caveat that magnitude and mass are not the same quantity. Blakeslee et al. (2006, hereafter B06) found that the mean and scatter in the color–magnitude relation of cluster early-type galaxies at $z = 0.83$ corresponded to a formation epoch of $z_{\star} = 2.2$ over a broad range of magnitudes, and therefore masses. Mei et al. (2009) found no evolution in the slope of the color–magnitude relation in cluster galaxies out to $z = 1.3$ extending the trend found with lower redshift clusters (Stanford et al. 1998; Holden et al. 2004). This is complementary to the results of Bell et al. (2004) and Ruhland et al. (2009) who found little evidence for evolution of the slope of the color–magnitude relation of field galaxies. A lack of evolution in the slope of the color–magnitude relation when, at the same time, lower mass galaxies are to apparently have lower mean M/L_B values is puzzling.

van Dokkum (2008, hereafter vD08) combined the M/L evolution and the evolution in the $U - V$ color of cluster early types to measure both the epoch of galaxy formation for massive galaxies and to constrain the slope of the IMF. Evolution in the colors of passively evolving stellar populations are governed by the location of the main-sequence turnoff, which is determined by the age of the stellar population. The rate of M/L evolution, however, is determined by the slope of the IMF at the turnoff as well as how bright the stars at the main-sequence turnoff are (Tinsley 1972). Thus, a slow pace of color evolution and a fast pace of M/L evolution, for example, can be explained by modifying the IMF. vD08 found, for the more massive cluster galaxies ($>10^{11} M_{\odot}$), a rapid pace of M/L evolution as compared to the color evolution. Thus, he concluded that the slope of the IMF at the main-sequence turnoff was flat, $x = -0.1$ instead of the usual Salpeter $x = 1.35$. This surprising result did not match previous measurements over the same redshift range made by other methods (Kelson et al. 2000c, 2001), a difference that could be explained by sample selection or the improved Maraston (2005) population synthesis models used by vD08. This result is also in conflict with some local indirect measurements of the IMF through lensing (e.g., Treu et al. 2010; Auger et al. 2010), though possible accommodation can still be made through variation in the dark matter halos properties. Because of the IMF, vD08 finds that the stars formed with a earlier formation epoch, $z = 3.7^{+2.3}_{-0.8}$. vD08 proposes a model that, by $z = 2$, predicts a more normal IMF. The rapid M/L evolution in the FP of lower mass galaxies implies that they should have formed at about $z = 1$–2. However, the lack of

evolution in the slope of the color–magnitude relation would imply an even steeper IMF slope for low-mass galaxies than vD08 found for the high-mass galaxies. This is in marked contrast to the expectations from the model of vD08 or other IMF slope measurements near $z = 2$ (Blain et al. 1999), both of which expect a more normal IMF for galaxies with masses $<10^{11} M_{\odot}$.

Because of the magnitude limits used for selection in previous work, computing the typical stellar age of formation for $<10^{11} M_{\odot}$ galaxies has been challenging. The highest M/L galaxies, those with the older populations, cannot be directly observed at $<10^{11} M_{\odot}$ and the impact of these galaxies must instead be included through a modeling process as was done in T05 or vdW05. We selected a sample of $z \simeq 1$ early-type galaxies in the field of MS 1054-03, a cluster of galaxies at $z = 0.83$ that samples much farther down the mass function. The main goal was to search for the more rapid evolution of the lower mass galaxies implied by the results of other efforts. A summary of the sample selection, and our measurements of the parameters for the FP, the effective radius (r_e), the average surface brightness within the effective radius ($\langle I_e \rangle$), and the velocity dispersion (σ) are discussed in Section 2. We determine the completeness of our sample in Section 3. Using these measurements, appropriately weighted, we measure the FP, color evolution, and the M/L_B evolution in Section 4. We use these measures to compute the typical star formation epoch of the stellar populations and comment on constraints of the IMF, in Section 5. Our results are summarized in Section 6. Throughout this paper, we assume $\Omega_m = 0.27$, $\Omega_{\Lambda} = 0.73$, and $H_o = 71$ km s^{-1} Mpc^{-1}.

2. DATA AND MEASUREMENTS

We have a sample of 59 galaxies in the field of the $z = 0.83$ cluster MS 1054-03 for which we have obtained spectra. Of these, 36 have dispersion measurements. For these galaxies, we have high-resolution imaging using the Advanced Camera for Surveys (ACS) on the *Hubble Space Telescope* (*HST*). Using the *HST*/ACS images, we measure the sizes and surface brightness by fitting elliptical Sérsic models to the data. The velocity dispersions are measured by fitting stellar templates broadened by the appropriate Gaussian line-of-sight velocity dispersions, representing the typical motion of stars inside the galaxies. Below we discuss in detail our observations and the resulting measurements.

2.1. $z = 0.83$ Sample Definition

We based our sample on a magnitude-limited survey of galaxies in the field of MS 1054-03. The original selection was done using a limiting magnitude of $J = 21.2$ mag (Vega) from a catalog of galaxies observed with the CFH12K at CFHT and the WIRC camera on the du Pont. Each galaxy in this sample had either a spectroscopic redshift, or a photometric redshift from a catalog of *BVRIJH* imaging data. Galaxies with spectroscopic redshifts were preferred in our selection. These photometric redshifts, the catalog construction, and the spectroscopic subsample will be discussed in a later paper.

Beyond meeting the J magnitude limit, the main criterion for selection was that the galaxy lies in the ACS field of view. We selected a DEIMOS mask center and position angle that maximized the number of galaxies with ACS imaging and with $J < 21.2$. A total of 44 galaxies met these criteria. Beyond our

main sample, 12 supplemental galaxies were selected to have $21.2 < J < 21.8$ and an additional 4 were targeted outside of the *HST* field of view. Also, we re-observed three galaxies that were in the sample of Wuyts et al. (2004, hereafter W04). Therefore, the total number of galaxies targeted for dispersions was 62.

We also combine our sample with that from W04. This earlier sample has a brighter *I* selection, see W04 for details, and used LRIS (Oke et al. 1995), with a smaller field of view than DEIMOS, for spectroscopic observations. The result is that the combined catalog of our sample and that of W04 will contain more galaxies in the inner regions of the cluster and will have a higher completeness at brighter magnitudes.

Our sample of galaxies is listed in Table A1 in Appendix A. We list our observed and rest-frame quantities along with the velocity dispersions. This table includes the sample of W04, which are identified by a "w" in front of the identification number.

2.2. HST/ACS Imaging

The ACS imaging used in this paper comes from two separate programs. The first, discussed in B06, used the F606W, F775W, and F850LP filters to image the center of the cluster. We will refer to the filters as V_{606}, i_{775}, and z_{850} for the rest of the paper. The second program imaged the outer regions of MS 1054-03 with the V_{606} and the F814W, or I_{814} filter. Example images can be seen in Appendix A, Figure A1.

We fit a model to each galaxy to determine the effective radius r_e and surface brightness $\langle I_e \rangle$ in the filter that most closely matches the rest-frame *B*. For the inner regions, this is the i_{775} filter while for those galaxies at larger radii, we used I_{814}. For each galaxy, we fit a model with a free Sérsic parameter constrained to fall within $1 \leqslant n \leqslant 4$ using GALFIT (Peng et al. 2002). For this paper, we use the best-fitting Sérsic parameters for r_e and $\langle I_e \rangle$, as this was shown to yield the same resulting FP as fixing $n = 4$ (Kelson et al. 2000a). When the best-fitting Sérsic n was at the limit of the allowed range, i.e., $n = 1$ or $n = 4$, we refit the image fixing n to that value.

The total magnitude we use is the normalization of the model fit. To measure colors, we used the circularized half-light or effective radius, $r_e = a_{hlr}\sqrt{q}$, where q is the ratio of the minor to major axis, or $1 - \epsilon$, and a_{hlr} is the half-light radius along the major axis of the best-fitting elliptical model as determined by GALFIT. This is the radius used both in our M/L analysis and the radius of the aperture for which we measured the galaxy's color, see B06 for details. From this circularized r_e, we compute the average surface brightness within that radius, or $\langle I_e \rangle$.

Using the simulation results of Holden et al. (2009), which placed real galaxy images in the ACS frames, we find that our measurements of the total magnitudes are too bright by -0.08 mag in the i_{775} data or -0.04 mag in the I_{814} data. We find a scatter of $\sigma = 0.07$ mag around the input magnitude for the simulations, after removing the offset, in good agreement with the expectations from total magnitude measurements in ACS imaging (Holden et al. 2005a). We apply this offset to our data in later sections.

In addition to fitting a bounded Sérsic model, we fit a fixed de Vaucouleur's model to our data so we can compare the two resulting fits. As expected, for galaxies classified as E or S0 the median best-fitting n value was $n = 3.6$ while, for those galaxies classified as spirals the median n was $n = 1.04$ (we discuss the classifications in the next section.) The n values showed a larger scatter for the spirals than for E and S0 systems as well. In cases where the best fitting $n > 3$, the values for r_e are good agreement with the $n = 4$ values, with differences of $11\% \pm 6\%$ on average. When best-fitting bounded Sérsic $n < 3$, the differences in the r_e are much larger, as expected (Kelson et al. 2000a).

2.2.1. Morphologies

Galaxy morphologies were obtained from the literature for all the galaxies in our sample. All of the morphologies were determined by Marc Postman from a *J* selected catalog with a limit of $J = 22.5$ mag. Each galaxy was classified in the passband closest to the rest-frame *B*, either the i_{775} or the I_{814}. The galaxies were classified in the same manner as those in Postman et al. (2005), and the galaxies in the central regions of MS 1054-03 were classified twice, once for this paper and once for the original Postman et al. (2005) study. The scatter for the fraction of E + S0 galaxies was 6%, the same as was found by using multiple classifiers in Postman et al. (2005). The morphologies, using the T system of Postman et al. (2005), are listed in Table A1. Galaxies with $T < 0$ are E and S0 systems.

2.2.2. Redshifted Magnitudes

We redshift the *U*, *B*, and *V* passbands to $z = 0.83$ and use the observed photometry to compute what magnitudes we would observe in these redshifted passbands. Hence, these passbands measure the flux densities at the redshifted effective λ for each filter; $\lambda_U(1 + z)$, $\lambda_B(1 + z)$, and $\lambda_V(1 + z)$. For brevity, we will call these redshifted magnitudes and label these magnitudes U_z, B_z, and V_z. With the removal of the additional dimming caused by the distance to the galaxies, these magnitudes would become rest-frame magnitudes. We compute these transformations between observed and redshifted magnitudes using a similar process as B06, Holden et al. (2006), and Holden et al. (2007), but based on the same basic approach as van Dokkum & Franx (1996) and Kelson et al. (2000a).

Both the i_{775} and I_{814} filters are mapped into B_z. We computed magnitudes at both $z = 0$ and $z = 0.83$ for a set of Bruzual & Charlot (2003, BC03) τ model templates. For the $z = 0$ filters, we used the *U*, *B*, and *V* curves from Buser (1978), specifically the B3 curve for the B_z as tabulated by BC03. We note that the transformations for the ACS passbands V_{606}, i_{775}, and z_{850} all match closely the transformations from B06. We explicitly note here that we do not attempt to use the BC03 templates to model the photometry directly. Rather, we use the templates to compute a grid of observed and redshifted magnitudes to which we fit a simple linear or quadratic relation.

The τ models used for the transformations span a range of parameters. These models had exponential time-scales of 0.1–5 Gyr, ages from 0.5 Gyr to 12 Gyr and three metal abundances, 2.5 solar, solar, and 0.4 solar. We then fit a linear or quadratic relation between the observed color or magnitude and the redshifted magnitude or color, for all models including all ages of those models. For the ACS transformations, we restricted the transformations to the range in colors we observed for galaxies at the redshift of the cluster and tabulate them in Table 1. All observed magnitudes use the AB system unless otherwise noted.

2.3. Spectral Observations

The spectral data were acquired over two observing runs in 2008 January and March, in excellent seeing and generally photometric conditions. The exposures were 20 minutes long

Table 1
Transformations from Observed to Redshifted Magnitudes

Filter[a] (mag)	Transformation (mag AB)	Color Range (mag AB)
r_z	$= J + 0.118(I - J) + 1.538$[b]	
B_z	$= i_{775} - 0.113(V_{606} - z_{850}) + 0.827$	$(V_{606} - z_{850}) < 1.5$
B_z	$= i_{775} - 0.190(V_{606} - z_{850}) + 0.964$	$1.5 < (V_{606} - z_{850}) < 2.6$
$(U - V)_z$	$= 0.876(V_{606} - z_{850}) - 0.757$	$(V_{606} - z_{850}) < 1.5$
$(U - V)_z$	$= 1.002(V_{606} - z_{850}) - 1.063$	$1.5 < (V_{606} - z_{850}) < 2.6$
B_z	$= I_{814} - 0.003(V_{606} - I_{814}) + 0.778$	$V_{606} - I_{814} < 1.2$
B_z	$= I_{814} - 0.006(V_{606} - I_{814}) + 0.783$	$1.2 < V_{606} - I_{814} < 2.4$
$(U - V)_z$	$= 1.135(V_{606} - I_{814}) - 0.861$	$V_{606} - I_{814} < 1.2$
$(U - V)_z$	$= 1.428(V_{606} - I_{814}) - 1.363$	$1.2 < V_{606} - I_{814} < 2.4$

Notes.
[a] Results are in Vega magnitudes for the UBV transformations, and we used the Buser (1978) filter curves. For the r_z, the magnitudes are AB and use the SDSS filter curves.
[b] The observed magnitudes are in the Vega system, unlike the other photometry in this table.

using the 600 line mm^{-1} grating on the DEIMOS spectrograph. The slits were 1″ wide, yielding a resolution of ~3.8 Å or an instrumental $\sigma = 60$ km s^{-1}. The slits were at least 8″ long, and between each exposure we offset the telescope by 2″ along the slit. Therefore, the object does not land on the same detector pixels in sequential exposures, but is instead offset by 2″. Each mask was observed for six exposures, or 2 hr. The final exposure was 16 hr for the deepest galaxies, 10 hr for the brighter objects.

2.3.1. Spectral Data Reductions

Our sky subtraction and spectral extraction used the techniques outlined in Kelson (2003) as implemented by D. D. Kelson. We used the internal quartz lamps to flat field the data. Wavelength solutions for each observation were determined using the night sky lines. Each slitlet has an independent sky model, see Kelson (2003) for details, which is then subtracted from each 20 minute observation.

Bright stars in each mask are used to measure the spatial offset between frames, as we offset the telescope between each exposure. After the sky model was subtracted from each frame, we then subtracted sequential frames to remove any residual sky signal. Each spectrum in each frame has a separate model used for optimal extraction (Horne 1986). The initial guesses for the profiles of the spectra are based on the bright stars in each mask, but are then fit to each spectrum in each exposure. The final one-dimensional spectrum is an extraction based on all of the separate exposures simultaneously, re-binned to the typical dispersion of the data, 0.64 Å pixel^{-1}. We plot example spectra in Appendix A, Figure A1.

2.3.2. Measuring the Velocity Dispersions

Velocity dispersions and high-precision redshifts are measured with a direct fitting method (see, e.g., Kelson et al. 2000b), as described by van der Wel et al. (2004) and vdW05, using a high-resolution solar spectrum that is smoothed and re-binned to match the galaxy spectra. If the continuum of the template and galaxy spectra are well matched, template mismatches from different spectral types introduce errors of, 2%–5%. This, combined with a small systematic uncertainty in the wavelength calibration and the possible non-Gaussian velocity distribution of the stars, prompts us to add in quadrature an empirically determined 5% error (see vdW05 for a fuller explanation) to the

formal fitting error on the measured velocity dispersion. Fitting in real space, as opposed to Fourier space, has the advantage that pixels can be weighted by the signal-to-noise ratio (S/N). In addition, we always mask regions that are affected by the atmospheric A and B absorption bands and emission lines. By default, we also mask Balmer absorption features, as these are unsuitable for velocity dispersion measurements. However, the Hϵ line, which is blended with the Ca H line, is not masked if Balmer absorption lines are weak, as is the case for the majority of the sample for which we managed to measure velocity dispersions (26 out of 39, including the three from Wuyts et al. 2004 that were re-observed). For the remaining 13 galaxies, Balmer lines are the dominant absorption features, such that we are forced to mask the Ca H and Hϵ blended line as well. The final velocity dispersions include a 6.6% aperture correction to give the central velocity dispersion within a fixed physical aperture of 1.6 kpc or 3″.4 at the redshift of Coma, the same aperture used by JFK96.

We note that thanks to the excellent quality of the spectra, only two galaxies out of the 55 targeted cluster galaxies with ACS imaging do not have measured velocity dispersions because of too low S/N in the continuum. For a further 14 galaxies, we cannot determine the velocity dispersion due to the lack of metal features, as their continua are either featureless (with emission lines) or dominated by strong Balmer absorption lines. These are all classified as late-type galaxies, in agreement with their spectral characteristics. Finally, one early-type galaxy has no measured velocity dispersion because of a moderate active galactic nucleus contribution. Because of this high success rate, we now have, for the first time, a high-redshift sample of early-type galaxies which spans a factor of ~4 in velocity dispersion and two orders of magnitude in dynamical mass. All galaxies with spectra are listed in Table A1, those without measured dispersions are so marked.

2.4. Low-redshift Comparison Sample

Our low-redshift comparison sample is a subset of the Coma sample from Holden et al. (2007). Each galaxy has surface brightness profiles fit to the Sloan Digital Sky Survey (SDSS) imaging data in the same manner as we have for MS 1054-03. Each galaxy is a member of the JFK96 E and S0 sample used in that FP study. We use the dispersions from JFK96 and the colors from Eisenhardt et al. (2007). The colors from Coma match the Bower et al. (1992) colors well, but cover a larger number of galaxies. We note here that we use only the half-light radius colors from Table 8 of Eisenhardt et al. (2007). For the total magnitudes, we use our values from the surface brightness profile fits to the SDSS images. The larger sample of sizes and colors allows us to expand on the sample of JFK96 which had B data for only a subset of all of the Coma galaxies with dispersions. We list in Table A2 the magnitudes, rest-frame colors and dispersions we use. Not all of the sample of JFK96 have colors listed in Eisenhardt et al. (2007) as noted in Table A2.

We use the same procedure and τ model population templates from BC03 as we used for the MS 1054-03, see Section 2.2.2, to transform the $z = 0.023$ observed U and V into $z = 0$ values U_z and V_z. We find that there is some curvature to the relation, and we require a quadratic fit of

$$(U - V)_z = (U - V) - 0.067(U - V)^2 + 0.220(U - V) - 0.220$$

to transform the observed magnitudes into the redshifted ones. For galaxies on the red sequence of Coma, we find $(U - V)_z =$
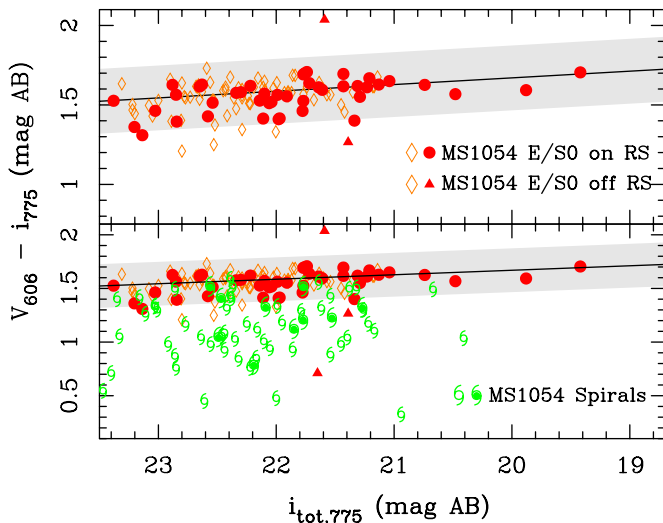
Figure 1. Color–magnitude relation for galaxies in the $z = 0.83$ cluster MS 1054-03 using *HST*/ACS data. We plot the $V_{606}-i_{775}$ color of galaxies as a function i_{775} magnitude, note different y-axis scale for top and bottom panels. Galaxies for which we have I_{814} data, we convert the I_{814} and $V_{606}-I_{814}$ data into the i_{775} and $V_{606}-i_{775}$ using the relations in Section 3.1. Larger red, filled circles and triangles are E and S0 galaxies with dispersions while smaller orange diamonds are E and S0 galaxies without dispersions. Green spirals are spiral or irregular galaxies, with filled spirals representing those with measured dispersions. We show, with solid lines, the color–magnitude relation of B06 while the gray regions shows the 3σ scatter. We will consider all galaxies within that shaded region as on the red sequence, those galaxies with dispersions that lie outside of that region are shown with filled triangles. We find a tight color–magnitude relation for the cluster E and S0 population in good agreement with the results from B06. This relation extends out to the E and S0 galaxies beyond the core of the cluster. We note that the statistical errors on the colors are smaller than the symbols used for plotting, see also B06.

(A color version of this figure is available in the online journal.)

$(U - V) - 0.04$ mag. Using the Coleman et al. (1980) elliptical model, we find $(U - V)_z = (U - V) - 0.04$ mag, in good agreement with our quadratic relation. We note that these values are significantly different from the $(U - V)_z = (U - V) - 0.00$ as found by Bower et al. (1992). For the rest of the analysis, we will use the second order equation above relating the observed $U - V$ and the $z = 0$ $(U - V)_z$ color.

3. DATA ANALYSIS

3.1. The Colors of the Galaxy Population

The colors of the galaxy population in MS 1054-03 have been studied extensively in B06. We show in Figure 1 the color–magnitude diagram of the population of galaxies that we targeted for dispersions in this study and the larger sample of galaxies that could have been targeted, a superset of the B06 sample. We note here that we remeasured the colors for all galaxies in our sample, instead of using the values from B06 and we will use these colors for our later measurements of the evolution of the cluster population.

Because two different programs observed MS 1054-03 which used two different sets of filters, we convert the colors and magnitudes of galaxies observed in I_{814} to i_{775} using the following relations

$$i_{775} = I_{841} + 0.248(V_{606} - I_{814}) - 0.211,$$

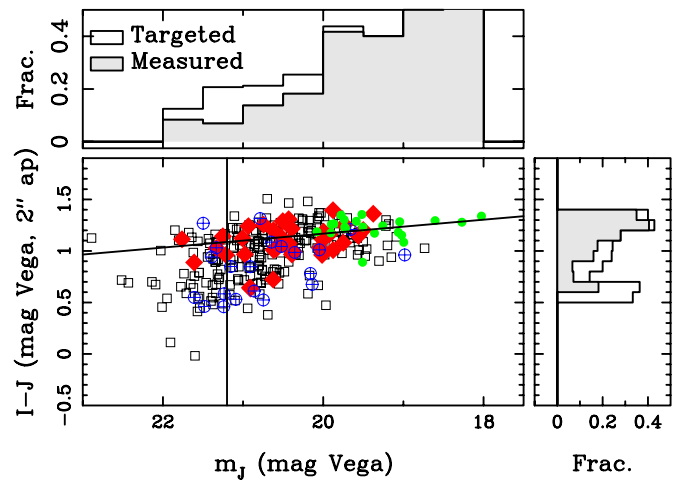$$V_{606} - i_{775} = 0.752(V_{606} - I_{814}) + 0.211,$$

Figure 2. Color–magnitude relation for the parent sample of galaxies in MS 1054-03. We plot the $I - J$ color of galaxies as a function J magnitude. The solid diamonds are the galaxies with measured dispersions from this paper while open circles with "+" symbols are galaxies we targeted but did not measure a dispersion for. Solid circles are galaxies with dispersions from W04. We show, as a vertical line, our magnitude limit of $J = 21.2$. The other line is the color–magnitude relation fit to the E/S0 population. Along the top, we show histograms of the fraction of galaxies with dispersions (filled gray) and targeted (open) as a function of J magnitude. This includes the galaxies from W04—or the solid circles—so this plot shows the relative weight of the different galaxies in our analysis. Along the right side, we plot the fraction of galaxies with dispersions and targeted with $J < 21.2$ by color. We find that our sample of galaxies with dispersions covers most of the range of colors and magnitudes in the parent sample. We successfully measure dispersions for $\sim 80\%$ of E/S0 galaxies and $\sim 50\%$ of spiral galaxies above our $J = 21.2$ magnitude limit that we targeted. Thus, 26% of all cluster galaxies in the ACS imaging and with $J < 21.2$ have dispersions, matching the visual impression of this figure. For 14 galaxies we targeted, we cannot determine the velocity dispersion due to the lack of metal features, as their spectra are either featureless (with emission lines) or dominated by strong Balmer absorption lines, producing a decreasing fraction of galaxies with bluer $I - J$ colors.

(A color version of this figure is available in the online journal.)

which are only valid between $1.2 < V_{606} - I_{814} < 2.4$. In Figure 1, we also removed galaxies from our sample that do not have spectroscopic redshifts.

Our colors significant a strong color–magnitude relation with a small scatter. The scatter for the whole sample of E and S0 galaxies with redshifts is $\sigma = 0.077 \pm 0.008$, larger than the scatter measured in B06. This larger scatter comes from the subsample of galaxies with $V_{606}-I_{814}$ colors that have been transformed into $V_{606}-i_{775}$ colors, removing them brings the scatter down to the size as measured in B06. This is consistent with the ~ 0.01–0.02 mag error typically found in these color transformations. We find we recover the slope and intercept from B06 with our larger sample, showing consistency between the two sets of measurements.

3.2. Success Rate

Evaluating the degree of evolution in the galaxy population requires calculating the completeness of our sample. Part of this is estimating how successful we are in measuring dispersions as a function of galaxy property. We targeted a total of 62 galaxies, with 44 above the magnitude limit of $J < 21.2$. Thirty-six have measured dispersions, with 31 above $J < 21.2$.

The simplest way of examining the completeness is to plot the distribution of galaxies with measured dispersions as a function size, color, and magnitude. First, we show the color–magnitude plot in Figure 2, followed by the size–magnitude relation in
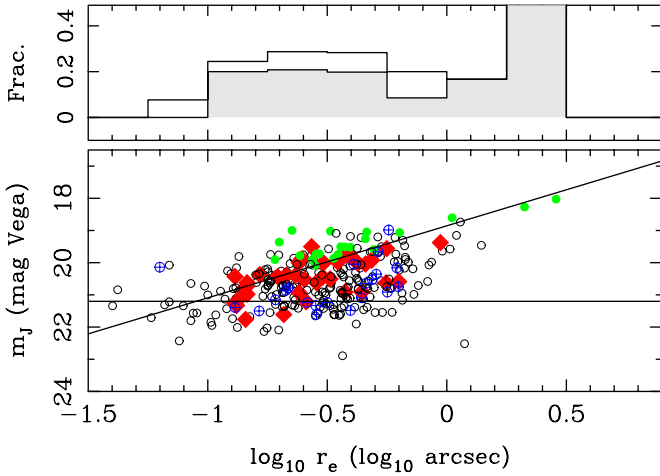
Figure 3. Size–magnitude relation for the parent sample of galaxies in MS 1054-03. We plot the J magnitude of galaxies as a function HST/ACS measured half-light radii using the same symbols as Figure 2. The fraction of galaxies with dispersions and $J < 21.2$ is plotted as a function of size in the gray histogram above the plot, and the fraction of galaxies targeted for dispersion measurements is shown with the open histogram. We find that fraction of galaxies with dispersions is relatively flat with size above our magnitude limit, with exception of the two brightest galaxies in the cluster and the smallest galaxies which are predominately below are magnitude limit. This means that we have no strong surface brightness selection bias. This is in accordance with previous work which finds that the S/N of a spectrum is proportional to $\langle I_e \rangle r_e^{1.9}$, which is close to $\langle I_e \rangle r_e^2$ or the observed magnitude (T05; van der Wel et al. 2008).

(A color version of this figure is available in the online journal.)

Figure 3. In both cases, the magnitude is the J, the selection passband.

3.2.1. The Success Rate of Measuring Dispersions for E and S0 Galaxies

We compute the fraction of galaxies with measured dispersions as a function of the magnitude and offset from the color–magnitude relation, shown in Figure 2. Our success in measuring velocity dispersions for E and S0 galaxies was high, with 29 dispersions out of the 34 galaxies targeted. The rate of success for measuring dispersions ranges from 100% at the brightest magnitudes to 70% for the galaxies below our magnitude limit $J = 21.2$, averaging $\sim$80% above our magnitude limit. When we look at galaxies as a function of I instead of J magnitude, we find a similar distribution. The fraction of galaxies targeted with measured dispersions is flat for $I < 22$ at 93%, dropping to 70% for the faintest $22.5 < I < 23$.

For E and S0 galaxies, we find no evidence of a size dependence on the success rate of measuring dispersions. This likely implies that magnitude is the important variable in deciding the success of a dispersion measurement. Both T05 and van der Wel et al. (2008) found that the signal to noise of a spectrum was predicted by the scaling of FP variables $\langle I_e \rangle r_e^{1.9}$, which is very close to magnitude of a galaxy, $\langle I_e \rangle r_e^2$.

3.2.2. The Success Rate of Dispersions for Early-type Spiral Galaxies

Our success with late-type galaxies is lower, with 10 measured dispersions out of the 20 targeted galaxies with $J < 21.2$, or 50% on average. We find that the success rate is flat with size and Sérsic index. It is also flat with magnitude, but only for galaxies $J < 21.2$. We measure no dispersions for the spiral galaxies below our $J < 21.2$ magnitude limit. The most important variable is the color, as we are biased toward

measuring the dispersions of red galaxies. Early-type spirals on the red sequence have a 100% success rate (see Figure 1 for our definition of the red sequence), while blueward of that, the rate drops to $\sim$30%. Because of this strong color dependence, we will give bluer spirals galaxies higher weight in our later analysis. Measuring the velocity dispersion requires the presence of strong metal lines, so we are biased against young or low-metallicity clusters in our sample. The small spiral fraction in MS 1054-03 for moderate mass galaxies (Holden et al. 2007) means the overall impact of this bias will be small.

3.3. How Representative is the Sample?

Thirty percent of the galaxies with $J < 21.2$ that could have been targeted had slits placed on them and 26% of galaxies with $J < 21.2$ have measured dispersions. These numbers, of course, depend mildly on the apparent magnitude of the galaxy.

The second sample we would like to consider is the published work of W04. W04 had a selection limit of $I = 22$ but preferentially targeted brighter galaxies, with more than half of the sample above $I \leqslant 21$ (or $J \leqslant 19.8$). This results in a sample with a much brighter effective magnitude limit. As can be seen in Figure 2, most of the galaxies that could have been targeted, and the ones that had been targeted, are on the red sequence.

Considering only E and S0 galaxies, our spectroscopic sample, combined with that of W04, targeted 38% of the galaxy population with $J < 21.2$, with 36% of E and S0 galaxies above $J = 21.2$ having dispersions. This combined sample of velocity dispersions represents a significant fraction of the E and S0 population in MS 1054-03. For the rest of the paper, we will use the completeness fraction of galaxies as a function of J magnitude as weights. The inclusion of the W04 sample makes these weights a strong function of magnitude, as can be seen in Figure 2. These completeness fractions range from 100% at the brightest magnitudes to 20% at our completeness limit of $J = 21.2$.

4. EVOLUTION OF THE FUNDAMENTAL PLANE AND GALAXY PROPERTIES

4.1. Fundamental Plane Evolution

4.1.1. Measuring the Tilt of the Fundamental Plane

We compute the parameters of the FP by fitting the $J < 21.2$ magnitude limited subset of our dispersions (σ), effective radii (r_e), and our B_z surface brightnesses. To fit the FP, $\log r_e = \alpha \log \sigma + \beta \log \langle I_e \rangle + \gamma$, where $\langle I_e \rangle$ is $-0.4\mu_B$, we minimized the mean absolute orthogonal deviation, as was done in JFK96:

$$\Delta = \frac{\log r_e - \alpha \log \sigma - \beta \log \langle I_e \rangle - \gamma}{\sqrt{(1 + \alpha^2 + \beta^2)}}$$

around the FP in all three projections, r_e, σ, and $\langle I_e \rangle$. We computed the average values of each of the coefficients for our final estimates of α, β, and γ. We estimated the errors on all of our fits to the FP by bootstrapping the data.

To compute the best-fitting plane, we need include our incompleteness. We did this two different ways. First, we use our weights we computed above in Section 3.3. Thus, galaxies at the fainter end of the luminosity function, closer to our limiting magnitude, get a higher weight. Second, we trim the data at a fixed value of σ. Because galaxies become intrinsically fainter at lower masses, by trimming at a fixed σ, we remove

Table 2
Summary of FP Parameters

Cluster	Limiting $\log \sigma$ (km s^{-1})	Morphology	α	β
JFK96[a]		E and S0	1.20 ± 0.07	-0.83 ± 0.02
Coma[b]	2.2	E and S0	1.18 ± 0.08	-0.78 ± 0.04
MS 1054-03	2.2	All	1.18 ± 0.16	-0.76 ± 0.06
MS 1054-03	2.2	E and S0	1.25 ± 0.11	-0.76 ± 0.03
MS 1054-03	2.1	All	1.19 ± 0.13	-0.78 ± 0.05

Notes.
[a] The best-fitting slopes for the B from the r selected Coma sample from Table 5 of JFK96.
[b] The best-fitting slopes as determined by for the Coma sample from Table A2 after selecting galaxies above the $\log \sigma$ limit and above the equivalent r magnitude limit that matches our J magnitude limit at $z = 0.83$.

the very lowest M/L galaxies where our sample will not have the corresponding high M/L galaxies at the same dispersion. We find that at $J = 21.2$, the typical dispersion is $\log_{10} \sigma = 2.10 \pm 0.10$, and thus we select limit of $\log_{10} \sigma = 2.20$. We will examine how our best-fitting plane varies depending on whether or not we remove the lowest σ galaxies or use our weights.

Our resulting best-fit values are summarized in Table 2 and, for comparison, we give the relations from JFK96 for the B selected sample. We verified that we recover the FP values from JFK96 when we fit to the values listed in Table A2.

When fitting the FP in MS 1054-03, at first we restricted the sample to only those galaxies that are E and S0 galaxies, a similar selection as JFK96, but using the $\log_{10} \sigma > 2.2$ and using the weights from above, we find $\alpha = 1.25 \pm 0.11$ and $\beta = -0.76 \pm 0.03$. The value of α is in good agreement with that of JFK96 but the value of β appears different at the level of two standard deviations. Hyde & Bernardi (2009) show that sample selection can cause large changes in the best-fitting slopes of the FP, and specifically trimming at a fixed σ. The JFK96 sample is complete to a fainter r limit than the equivalent J limit for our sample and did not have a limiting σ as we did. So, we restricted the sample of Coma galaxies to those galaxies that would match our high-redshift selection criteria, namely, E and S0 galaxies with an equivalent r selection corresponding to our $J < 21.2$ at $z = 0.83$ and the same limiting σ. We refit the FP for the Coma sample, and we find that value of β for the Coma galaxies decreases to $\beta = -0.78 \pm 0.04$ with α unchanged. Thus, we conclude that the mild difference in β we find in comparison to JFK96 is likely a result of sample selection, and that there is no evolution in the tilt of the FP.

Including early-type spirals in our sample does not change the result significantly, as was seen in a $z = 0.33$ cluster by Kelson et al. (2000c). Fitting the FP to all galaxies with $\log_{10} \sigma > 2.2$ and using the weights from above, we find $\alpha = 1.18 \pm 0.16$ and $\beta = -0.76 \pm 0.06$. Lowering the limiting σ to $\log_{10} \sigma > 2.1$ and using the weights from above, we find $\alpha = 1.19 \pm 0.13$ and $\beta = -0.78 \pm 0.05$. In general, these numbers are in good agreement with the values for a more restrictive subsample of E and S0 galaxies with $\log_{10} \sigma > 2.2$. This shows that our results are robust to different limiting velocity dispersions and uncertainties in the sample selections.

From these tests, we conclude that the observations are consistent with an unchanging tilt in the FP. In Figure 4, we plot the FP for our $z = 0.83$ sample. We use the values of α and β from JFK96 to plot both the low- and high-redshift samples.
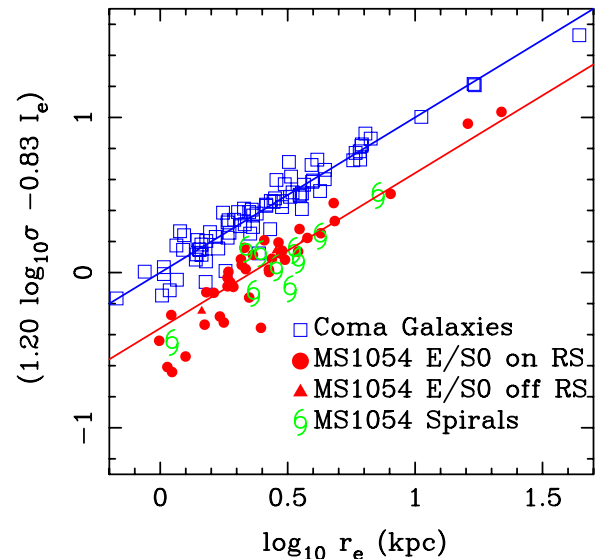

Figure 4. Fundamental plane for the Coma sample of JFK96 (blue open squares) and our sample in MS 1054-03. Spirals are marked by green spiral symbols while E and S0 galaxies are filled red points, circles for those on the red sequence and triangles for those off. We plot all the galaxies in Coma, regardless of σ or r magnitude. We use the values of the slope of the FP, $\alpha = 1.20$ and $\beta = 0.83$, from JFK96, and plot the FP relation as a blue solid line for Coma. The red solid line is the FP relation for MS 1054-03 using the same slope as we do for Coma, but with an offset to match the relation in MS 1054-03. We find no evidence that the tilt in the FP evolves, as we recover the relation of JFK96 for the galaxies in our sample. We do find that the FP has a different zero point. The change in the zero point is $\Delta \log_{10} r_e = -0.38 \pm 0.02$, which corresponds to evolution of $\Delta \log_{10} M/L_B = -0.44 \pm 0.03$ for the stellar populations of the cluster galaxies.

(A color version of this figure is available in the online journal.)

4.1.2. Residuals around the Fundamental Plane

vv07 found that there was a strong correlation between the residuals around $\log r_e$ and other quantities related to the mass of the galaxy, such as σ or the dynamical mass. Such a deviation could be caused by curvature in the FP and is more thoroughly explored in van der Marel & van Dokkum (2007a, 2007b). We assume the FP relation from JFK96 and we plot, in Figure 5, the deviation between the measured r_e and the predicted r_e from the FP as a function of r_e, σ, and the dynamical mass $M_{\rm dyn}$. We computed $M_{\rm dyn}$ is in $M_\odot$ using the relation $M_{\rm dyn} = 5\sigma^2 r_e / G$ or

$$\log_{10} M = 2 \log_{10} \sigma + \log_{10} r_e + 6.07$$

with σ is in km s^{-1} and r_e is kpc. We find galaxies with dynamical masses $M_{\rm dyn} < 10^{11} M_\odot$ that lie close to the $z = 0$ relation after adjusting for passive M/L evolution (see below). This result is expected given the lack of evolution we find in the tilt of the FP.

4.1.3. M/L Evolution from the Offset of the Fundamental Plane

Traditionally, the offset in the FP is used to measure the amount of M/L evolution. This is done by assuming that the offset, the value of $\Delta \log_{10} r_e$, is all caused by luminosity evolution, or a change in $\langle I_e \rangle$. If we take the value we measure, $\Delta \log_{10} r_e = -0.38 \pm 0.02$, in Figure 5 we find $\Delta \log_{10} M/L_B = -0.44 \pm 0.03$ or $d \log_{10} M/L_B = -0.60 \pm 0.04 \, dz$. Our values are in excellent agreement with the value of $\Delta \log_{10} M/L_B = -0.415 \pm 0.040$ at $z = 0.83$ as found by vv07 but much smaller than the $d \log_{10} M/L_B = -0.72^{+0.07}_{-0.05} dz$ of T05.
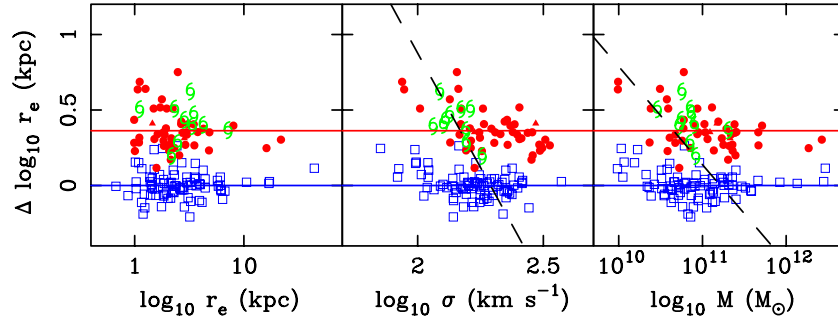
Figure 5. Deviations from the fundamental plane of JFK96 as a function of r_e, σ, and mass ($M_{\rm dyn} = 5\sigma^2 r_e/G$). We use the same symbols as in Figure 4 and show the approximate $J = 21.2$ selection limits for a red-sequence galaxy at $z = 0.83$ with dashed lines. Galaxies below those lines are in our fainter subsample ($21.2 < J < 21.8$). The average offset of the fundamental plane, $\Delta \log_{10} r_e = -0.38 \pm 0.02$ (which corresponds to $\Delta \log_{10} M/L_B = -0.44 \pm 0.03$), is illustrated with a red line. The offset of $z = 0.83$ galaxies from the $z = 0.023$ fundamental plane is not larger for galaxies with low σ or mass as long as they lie above our limiting magnitude, as expected if the slope or tilt of the fundamental plane does not evolve.

(A color version of this figure is available in the online journal.)

4.2. Evolution in M/L from the Virial Estimator

We can combine our measurements of the total B light with the M to estimate a M/L_B value or

$$M/L_B = 5\sigma^2/(2\pi G r_e \langle I_e \rangle).$$

We show in Figure 6 the relation between M/L_B and σ for Coma and our sample of galaxies in MS 1054-03 from the virial M/L estimator. We fit the results at both low and high redshifts using a robust linear fitting technique that minimizes the median absolute deviation and estimate our errors with bootstrapping. The bootstrapping is performed in a weighted manner, based on the weights determined in Section 3.3. It appears that the slope has not evolved between the low- and high-redshift samples. In our sample of galaxies in MS 1054-03, we find for the Coma sample, $M/L_B \propto \sigma^{0.98 \pm 0.10}$, in excellent agreement with the low-redshift result of van der Marel & van Dokkum (2007b), while for our sample in MS 1054-03 we find $M/L_B \propto \sigma^{1.12 \pm 0.21}$. If we assume no change in the slope, we find $\Delta \log_{10} M/L_B = -0.50 \pm 0.02$ at a fixed σ for the whole of the galaxy population with $J < 21.2$. For the red sequence, E and S0 population, we find $\Delta \log_{10} M/L_B = -0.50 \pm 0.03$, or no measurable difference.

Our measured M/L_B evolution using the virial estimator is higher than the $\Delta \log_{10} M/L_B = -0.44 \pm 0.03$ we find in Section 4.1. In principle, these results should be the same if the evolution in the FP is caused entirely by M/L evolution. van der Marel & van Dokkum (2007b) showed that structural evolution, such as caused by higher rotation rates or size evolution, would cause the disagreement we observe between the two estimators of M/L_B evolution. van der Marel & van Dokkum (2007b) find, for their sample, that the virial estimator yields a result closer to the M/L as estimate by the dynamical modeling done by van der Marel & van Dokkum (2007b). For the rest of this paper, we will use the virial estimator as a consequence, but will note how using the FP results changes our results. This should avoid some of the bias found in Saglia et al. (2010). Finally, we add that van der Wel & van der Marel (2008) found little evidence for higher rotation rates in field E and S0 galaxies, thus evolution in rotation alone does not explain the results of T05 or vdW05.

4.3. Color Evolution

In Figure 7, we show that, as expected, the rest-frame $(U-V)_z$ colors of the MS 1054-03 galaxies are bluer than the colors of the
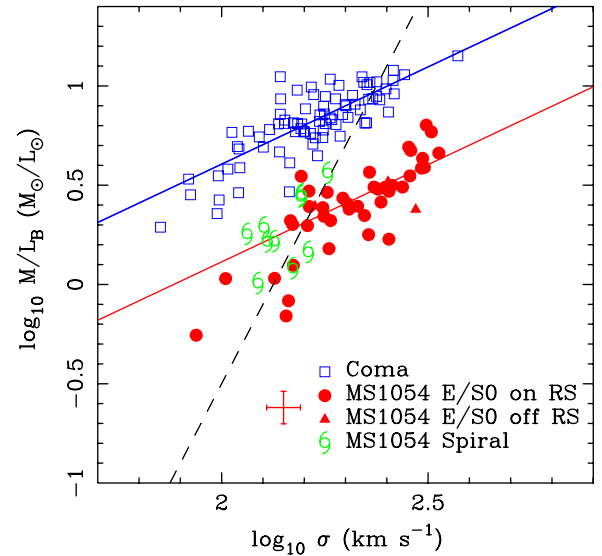
Figure 6. M/L_B as measured by the virial estimator ($M/L_B = 5\sigma^2/(2\pi G r_e \langle I_e \rangle)$) vs. σ for the samples of Coma and MS 1054-03. We use the same symbols as in Figure 4. The black dashed line is the approximate selection limit for a red-sequence galaxy in MS 1054-03. We show the typical errors for MS 1054-03 in the lower right. Our high-redshift slope is compatible, within the errors, with the slope we find at low redshift. We find a relation of $\log_{10} M/L_B = 0.98 \log_{10}(\sigma/200 \text{ km s}^{-1}) + 0.90$ for Coma (shown as a blue line) and offset of $\Delta \log_{10} M/L_B = -0.50 \pm 0.03$ for red E and S0 galaxies in MS 1054-03 (shown as a red line) and $\Delta \log_{10} M/L_B = -0.50 \pm 0.02$ for the whole sample of $J < 21.2$ galaxies, regardless of color or morphological type.

(A color version of this figure is available in the online journal.)

Coma galaxies. This shift can be seen both at fixed luminosity and at fixed σ. Since σ is expected to evolve little or not at all as compared to luminosity, we adopt the color evolution at fixed σ as the quantify of interest. For Coma, we find the relation $(U-V)_z = 0.653 \pm 0.093 \log_{10}(\sigma/200 \text{ km s}^{-1}) + 1.475 \pm 0.015$.

We find no evolution in the slope, as expected from the larger survey of Mei et al. (2009) which found no change in the slope of the color–magnitude relation for eight $z > 0.8$ clusters. We measure the offset in the average color for all red-sequence E and S0 galaxies in our sample with $\log_{10}(\sigma) > 2.2$ and we find $\Delta(U-V)_z = -0.24 \pm 0.02$ mag between $z = 0.831$ and $z = 0.023$. As above, we use bootstrapping to estimate the errors on the color–σ relation in Coma and on the amount of color evolution.

Figure 7. Redshifted color–magnitude and color–σ relations. We show the $(U - V)_z$ colors both for Coma galaxies ($z = 0.0231$) and galaxies in MS 1054-03 ($z = 0.831$). We use the same symbols here as in Figure 1. The typical error in the color and σ is shown, as a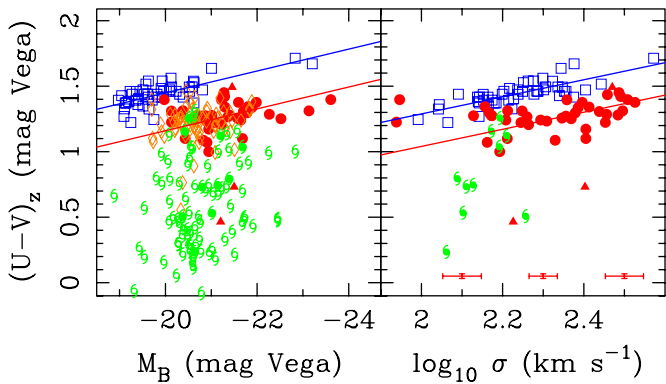 function of σ, across the bottom of the right panel. We note that the large σ sample is dominated by W04 which have larger errors in σ owing to shorter effective exposure times. We find evolution in the offset of the color–magnitude relation and the color–σ relation, which implies a younger population at higher redshift. This evolution is determined by fitting the color–magnitude and color–σ relation to the Coma galaxies, with the relations shown as blue lines, and then computing the best-fitting offset for those galaxies on the red sequence in MS 1054-03. The relations for MS 1054-03 are shown as red lines. We find no statistically significant evidence for a change in the slope of either relation when we fit for them to red-sequence cluster members. For all red-sequence E and S0 galaxies in our sample with $\log_{10}(\sigma) > 2.2$, we find $\Delta(U - V)_z = -0.24 \pm 0.02$ mag of color evolution.

(A color version of this figure is available in the online journal.)

5. THE EPOCH OF CLUSTER GALAXY FORMATION

We use a combination of the M/L_B evolution and the $U - V$ color evolution to estimate the median epoch of star formation for galaxies in our cluster sample. We estimate the luminosity-weighted age of the stellar populations by computing which single stellar population from Maraston (2005, hereafter M05) best reproduces both M/L_B and $U - V$ evolution we observe. We will assume that the populations are coeval and we include all galaxies, regardless of morphological type, in MS 1054-03. Fitting both the M/L_B evolution and the color evolution simultaneously, we find that M05 models with a solar abundance prefer $z_\star = 1.8^{+0.2}_{-0.2}$. Because of our completeness limits, this is in effect the median age of formation for galaxies with $\log_{10} \sigma > 2.2$ or, roughly, a dynamical mass of $M > 6 \times 10^{10} M_\odot$.

If we use the smaller M/L from the offset in the FP, see Section 4.1, we find a higher formation redshift, $z_\star = 2.0^{+0.2}_{-0.2}$, though well within the range of the errors. In fact, the uncertainties in this are as much from the assumptions about the stellar populations as from the errors on the measurements. For example, assuming a metallicity $\log Z/Z_\odot = 0.35$ increases the formation epoch to $z_\star = 2.5^{+0.3}_{-0.2}$. We note that the pace of M/L evolution and the pace of the $U - V$ evolution are in mild disagreement with expectations of a higher metallicity population, but if we assume the slower pace of evolution from the offset of the FP, we find a better agreement, though we prefer the estimate from the virial M/L estimator for reasons discussed in Section 4.2.

There are significant differences between the models of BC03 and those of M05, but these are in how the models address the post-main-sequence evolution, specifically the thermally pulsating asymptotic giant branch stars. This can cause significant differences in the near-IR fluxes, but as was shown in van der Wel et al. (2006) the impact on the M05 predictions for the optical properties of older stellar populations is small. We esti-

mated the typical epoch of formation for the whole sample using the BC03 models and found $z_\star = 1.6^{+0.2}_{-0.1}$, in good agreement with the value of $z_\star = 1.8^{+0.2}_{-0.2}$ found using M05 with the same assumptions.

From the above results, we conclude that the epoch of formation for the galaxies in MS 1054-03 is $z_\star = 2.0 \pm 0.3 \pm 0.3$ (sys), in good agreement with the results from vv07 for their sample of higher mass ($>10^{11} M_\odot$) galaxies. The systematic error shows the range of allowed values given both the uncertainties in the stellar population models as well as the possible different M/L values.

5.1. Constraints on the Initial Mass Function

The evolution of M/L for passively evolving systems depends critically on the IMF, while the evolution in optical colors depends less so (Tinsley 1972). This comes about because both the colors and luminosity of a passively evolving stellar population are determined by the properties of the stars at the main-sequence turnoff. The color evolution depends mostly on the effective temperature of those stars, and thus is most strongly influenced by the age and typical metallicity. The luminosity evolution, however, depends on not just luminosity of the individual stars, but the relative numbers of stars as a function of mass. Thus, our measurements of the ratio of the pace of color and luminosity evolution can be used to constrain the IMF of stars at the main-sequence turnoff, around 0.8–1.0 $M_\odot$ for old stellar populations in our target galaxies.

vD08 found that, for cluster galaxies with masses $>10^{11} M_\odot$, the color and M/L evolution favored an IMF very different from a Salpeter slope in the mass range of 0.8–1.0 $M_\odot$. The assumptions we made in the previous section use a Salpeter-like IMF to estimate the formation epoch from the M/L evolution. vD08, however, shows that the IMF that most closely agrees with the sample in that paper yields a formation epoch of $z_\star = 3.7^{+2.3}_{-0.8}$ for cluster galaxies with $>10^{11} M_\odot$. In light of the results of vD08, we have examined our data removing the assumption of a fixed IMF.

vD08 provides a useful relation for constraining the IMF with the evolution in the color and M/L_B. vD08 finds that for solar metal abundances with the M05 models with ages >1 Gyr

$$2.5 \frac{\Delta \log(M/L_B)}{\Delta(U - V)} = 6.93 - 1.81x,$$

where the terms $\Delta \log_{10}(M/L_B)$ and $\Delta(U - V)$ represent the amount of evolution in the M/L_B and color, respectively. The term x is the slope of the IMF, where the Salpeter (1955) value is $x = 1.35$.

We plot $\Delta \log_{10} M/L_B$ and $\Delta(U - V)$ along with the expected evolution in $\Delta \log_{10} M/L_B$ and $\Delta(U - V)$ in Figure 8. We find that our data are in mild disagreement with the expected evolution from a Salpeter IMF, with a slope of IMF better described by $x = 0.9 \pm 0.2$, shown in Figure 8 with a red line. This is a difference of 2.25 standard deviations from the Salpeter value of $x = -1.35$. This value modestly changes the best-fitting formation epoch from $z_\star = 1.8^{+0.2}_{-0.2}$ to $z_\star = 2.0 \pm 0.3$. As we discuss above, such a shift is in line with the other systematic uncertainties.

5.1.1. Contrasting Our Results with vD08

vD08 found much lower values for x, with a preferred value of $x = -0.1$ for galaxies with a solar metallicity. We find $x = 0.9 \pm 0.2$ in large part because we compare only Coma and
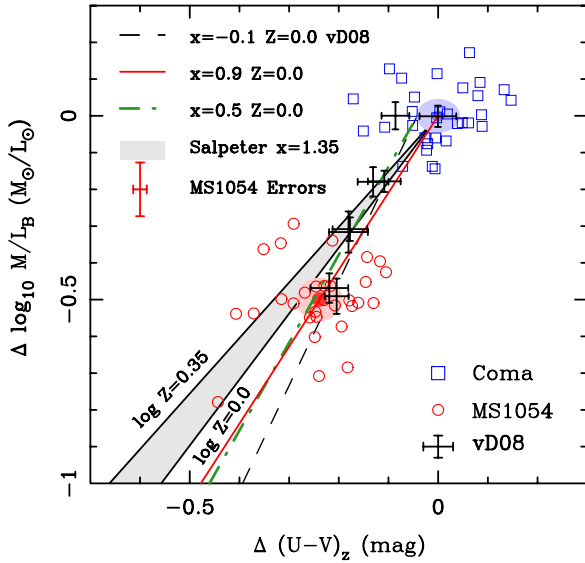
Figure 8. $\Delta \log_{10} M/L_B$ vs. $\Delta(U - V)_z$ for our Coma E and S0 sample (blue squares) and for the red-sequence E and S0 galaxies in MS 1054-03 with $\log_{10} \sigma > 2.2$ (red, open circles). For each galaxy, we measure the offset with respect to the Coma M/L_B–σ (Figure 6) and $U - V$–σ (Figure 7) relations. Our mean offsets in $\Delta(U - V)_z$ and $\Delta M/L_B$ with 1σ error in red and 3σ in lighter pink, with our corresponding 1σ and 3σ error ellipses for Coma in dark and light blue, respectively. The typical individual errors for MS 1054-03 are shown by a red error bar in the lower right. We show the expected evolution in $\Delta \log_{10} M/L_B$ vs. $\Delta(U-V)_z$ for an IMF with a Salpeter slope at $\sim$0.8–1.0 $M_\odot$ with a metallicity ranging from solar to more than twice solar, $\log_{10}(Z/Z_\odot) = 0.35$, in the filled gray region. The best-fitting IMF slope, $x = 0.9 \pm 0.2$ from *only* our data is shown by the red line. Our sample, alone, shows only tentative evidence of a shift in the IMF, at the level of 2.25 standard deviations. The black error bars are the data from vD08, with the expected evolution from the best-fitting IMF of vD08, $x = -0.1$, shown as a dashed line. Using the lower redshift data set of vD08, namely, Coma and A2218, we would find $x = 0.5 \pm 0.2$, shown as a green dash-dotted line. The general agreement with our results (in color) and those of vD08 (in black), however, implies that both samples are drawn from similar parent samples. From this, we conclude that the stellar populations should have similar IMF slopes.

(A color version of this figure is available in the online journal.)

MS 1054-03. If we include the lower redshift data from vD08, specifically the data from A2218, we would find a shallower slope of $x = 0.5 \pm 0.2$ illustrated with a green dash-dotted line in Figure 8. The key difference between our result and those of vD08 is not in our high-redshift data, but rather the lower redshift sample.

vD08's galaxy samples were selected by including all galaxies with dynamical masses $>10^{11} M_\odot$. This is in contrast to our sample in MS 1054-03, which is limited to those galaxies at $\log_{10} \sigma > 2.20$, roughly $6 \times 10^{10} M_\odot$. If we instead use the criteria of vD08, namely, a subsample of E and S0 galaxies in MS 1054-03 with $>10^{11} M_\odot$, we find a $\Delta U - V = 0.22 \pm 0.04$, similar to the $\Delta U - V = 0.20 \pm 0.04$ found in vD08 and 0.03 mag smaller than the offset we measure for the full sample of galaxies in MS 1054-03. So part of the difference in our derived slope of the IMF comes from our sample probing a larger mass range. This sample selection results in a difference in $\Delta U - V = 0.03$ mag or a slope of $x = 0.5 \pm 0.2$ instead of $x = 0.9 \pm 0.2$. The rest of the difference between our value of $x = 0.9 \pm 0.2$ from our data alone and the $x = -0.1$ as measured by vD08 is the larger sample of low-redshift clusters that vD08 used. If we use the same mass selection as vD08, all E and S0 galaxies with $>10^{11} M_\odot$ and use the low-redshift sample of Coma and A2218, we recover the $x = -0.1$ found by vD08.

The data we have used in this paper have been analyzed in a consistent manner throughout. vD08 used a larger set of data from the literature that was made as consistent as possible (see van Dokkum & van der Marel 2007 for details). In vD08, it can be seen, both by examining the equivalent of Figure 8 from that paper or from other measurements of the color and M/L evolution, that the low-redshift data are as important to the conclusions as the high-redshift data, a result reinforced by the change in the slope of the IMF we find when we include the eight galaxies of A2218. Because of this, the large samples of low-redshift FP samples, such as Hyde & Bernardi (2009), should be used to more fully explore joint evolution in M/L and color. From this, we will have a much more solid measurement of the IMF for E and S0 systems.

5.2. Implications from the Lack of Evolution in the Tilt of the Fundamental Plane

We find no evidence for any evolution in the tilt of the FP, nor do we find evidence for a change in slope of the color–σ relation. Therefore, our data would rule out the scenario where the median star formation epoch depends strongly on galaxy mass. We quantified this by fitting a model to the color and M/L data in both Coma and MS 1054-03. This model assumes that the galaxies in Coma and MS 1054-03 are coeval and have the same metal abundance, and leaves the scatter as a free parameter at each redshift. The model parameterizes the formation epoch as power-law function of the σ, $t_f = t_o(\sigma/160 \text{ km s}^{-1})^\alpha$. Fitting this model to those galaxies above our magnitude and σ limit, we find $\alpha = 0.2^{+0.15}_{-0.1}$ and recover a t_o corresponding to $z_\star = 1.5$. The low value for α means that, in our best-fitting model, the most massive galaxies ($\log_{10} \sigma = 2.5$) have a $z_\star = 2.3^{+1.3}_{-0.3}$. Our resulting value for α is on the small side of those reported in the literature, which we will discuss in later, in Section 5.4.

There is an important caveat to this analysis. We assume that the whole population in both clusters is coeval. Because the cluster population grows by accretion of galaxies from outside of the cluster, however, the population of galaxies in MS 1054-03 represents only a subset of the $z = 0$ cluster galaxy population. Thus, we would overestimate the epoch of cluster galaxy formation as we would only include those galaxies that are already E, S0 or early-type spirals at $z = 0.83$. If this process is dramatic, we would expect to find rapid evolution in the fraction E and S0 galaxies in clusters. However, for mass-selected samples, the amount of observed evolution in the fraction of E and S0 galaxies is minimal (Holden et al. 2006, 2007). van Dokkum & Franx (2001) provide a method for calculating the impact of this bias. We find if we assume that 90% of the galaxies were in our sample at $z = 1$, there is no shift in the epoch of formation. Assuming that fraction is only 50%, the effective epoch of formation shifts downward by $\Delta z = 0.2$, $z_\star = 1.4$ for galaxies with $\log \sigma = 2.2$. It is likely that this fraction actually varies with velocity dispersion, so, in effect, the actual slope of the relation between formation epoch and dispersion is mildly steeper than we measure. If we assume that 50% of the $\log \sigma = 2.2$ galaxies were not present in the sample while 90% of the $\log \sigma = 2.5$ were present, this shifts the resulting α from $\alpha = 0.2^{+0.15}_{-0.1}$ to $\alpha = 0.25^{+0.15}_{-0.1}$, a very modest change.

5.2.1. Implications for the IMF

Renzini (2006) shows that a trend in the IMF with mass would cause the tilt in the FP to evolve with redshift. Because our measured slope of the FP changes little, if at all, we can

immediately conclude that the IMF of the lower mass galaxies in our sample is similar to that of the higher mass systems. In Section 5.1, we show that most of the difference between the slope of the IMF from our sample, $x = 0.9$, and the slope of the IMF as determined by vD08, $x = -0.1$, comes from the larger sample of clusters used in vD08. The remaining difference, a change in the slope $\Delta x = 0.4$, comes about from our sample of lower mass galaxies in MS 1054-03. Thus, the IMF for cluster galaxies has, at most, a mild mass dependence for galaxies with $\log_{10} \sigma > 2.2$, and a mass dependence that appears in agreement with the results of Treu et al. (2010).

As many lower mass cluster galaxies must have formed in more field-like environments before falling into the cluster (e.g., Patel et al. 2009b; Berrier et al. 2009, and references therein), then the IMF for many field E and S0 galaxies should be similar to what is found for cluster galaxies at similar masses. This follows regardless of whether the conclusions of vD08 are correct or, in contrast, the conclusions of Treu et al. (2010) are correct. Therefore, if there is a different IMF for E and S0 galaxies, it should be prevalent in all moderate to high-mass galaxies regardless of environment.

5.3. Comparison with Color Measurements

A number of color-based measurements of the formation epoch of cluster galaxies have been made. B06 found that the scatter in the colors in MS 1054-03 and another $z = 0.83$ cluster, RX J0152-13, implied a star formation epoch of $z_\star \simeq 2.2$, in good agreement with our results. Mei et al. (2009) found a similar scatter in the colors of the E and S0 population in a sample of eight clusters, including the two in B06, indicating a similar formation epoch for the $z \sim 1$ cluster population. Holden et al. (2004) measured $z_\star = 3^{+2}_{-1}$ by fitting the evolution of the zero point of the color–magnitude relation of E and S0 galaxies, as opposed to the scatter as was done in B06, for a sample of 24 clusters spanning a redshift range of $0.3 < z < 1.3$. Eisenhardt et al. (2008) and Mancone et al. (2010) find a similar formation epoch for the galaxies on the red sequence in a much larger sample of $z > 1$ clusters than in Holden et al. (2004). All of these results all point to $z = 2$–3 being the important epoch for the star formation of cluster early-type systems. Interestingly, Eisenhardt et al. (2008) find evidence that the average formation epoch of the cluster red sequence increases for the higher redshift cluster galaxies, the expected result if more galaxies are joining the red sequence over time.

At $z \sim 2$–3, Brammer & van Dokkum (2007), Zirm et al. (2008), Kriek et al. (2008), and Brammer et al. (2009) all find a well-defined red sequence in both clusters and the field environment. These early-type systems have finished forming their stars at $z \sim 3$, a time higher than the mean age as measured by colors or by the FP. However, these galaxies represent only the oldest 10% of the early-type population, and so are consistent with a more typical epoch of $z_\star \sim 2$ for the majority of the population. Therefore, color measurements show that $\sim L^\star$ galaxies have stellar populations with formation times of $z_\star \sim 2$–3, an epoch when a sizable fraction of the stars that exist today were formed and entirely consistent with our FP measurements.

5.4. Comparison with Archaeological Studies of Present-day Galaxies

Trager et al. (2000a, 2000b) found that age and dispersion were part of a hyper-plane also including metallicity and α enhancement. In general, higher dispersion galaxies have older population ages at a fixed metallicity and galaxies in denser environments show older ages. A number of papers have built on these results, finding a strong correlation between the properties of stellar populations and velocity dispersions of galaxies for very large samples (Nelan et al. 2005; Gallazzi et al. 2006; Graves et al. 2009a, 2009b; Smith et al. 2009). Interestingly dynamical mass is not the important variable, rather Graves et al. (2009a, 2009b) and Smith et al. (2009) both found that σ is the driving parameter for determining the stellar populations of $z = 0$ early-type galaxies.

The ages derived from these measurements are strikingly young for lower dispersion galaxies, roughly 30%–50% of galaxies at $\log_{10} \sigma = 2.2$ having formation ages corresponding to $z \sim 0.8$. Trager et al. (2008) found similar results for E and S0 galaxies in the Coma cluster, a typical age of 5–8 Gyr, or roughly a $z_\star \sim 0.5$–1, regardless of galaxy mass. Correspondingly, many authors find a steep relation between the age of the stellar population and velocity dispersion, with logarithmic slopes of 0.4–0.6 common (Trager et al. 2000a; Nelan et al. 2005; Smith et al. 2009) and values up to ~ 1.1 found (Bernardi et al. 2003b). Kelson et al. (2006) found a strong relation between metallicity and σ, but, in contrast, that after accounting for the selection limits the population of CL 1358+62 showed no age variation with σ.

Part of the reason for the difference in our results, a shallow age–dispersion relation, and the steeper ones found by others come about from our use of broadband photometric data as compared to fitting models of stellar populations to spectra. Tortora et al. (2009) found that the slope of the age–σ relation is much shallower when stellar populations are fit to only broadband photometry. La Barbera et al. (2010a) finds, when analyzing a sample of $0.05 < z < 0.95$ early-types, that there is little change in the ages of stellar populations with mass when the ages are determined by the FP in different passbands. Further, Cooper et al. (2009) found that galaxies in high-density environments with the same broadband color and magnitude as galaxies in low-density environments, had both larger ages and larger metallicities using models fit to spectra from Gallazzi et al. (2006). This shows that the population parameters derived from spectra are not the same as those derived from color measurements alone. Trager & Somerville (2009) provide a potential framework to interpret these seemingly contradictory results. Trager & Somerville (2009) find that the ages that result from fitting simple stellar population models to spectral features are likely when the last 5%–10% of the stars formed. Thus, these young apparent ages are not when the median star was formed, but rather the epoch when the last star formation occurred.

5.5. The Field versus the Cluster Early-type Population

Our sample consists entirely of cluster galaxies, so part of the reason we find a different result from field samples such as T05 or vdW05 could simply be environment. Bernardi et al. (2003a), Bernardi et al. (2006), Cooper et al. (2009), La Barbera et al. (2010b), and Saglia et al. (2010) all find differences in the FP or the stellar populations of galaxies such that galaxies in clusters appear older than the same mass field galaxies.

Interestingly, T05 show, in Figure 14 of their paper, that most massive ($> 10^{11} M_\odot$) galaxies have a formation epoch of $z \sim 2$–3. vv07 perform a separate analysis and find a similar result. The main differences between our results and T05 are at $< 10^{11} M_\odot$. We find that $\sim L^\star$ cluster galaxies have a typical formation epoch of $z_\star = 1.7$ to $z_\star = 2$, whereas

T05 find $z_\star \sim 1.2$ for similar mass galaxies in their sample. In our MS 1054-03 sample, we have galaxies that show rapid enough M/L evolution to be consistent with a formation epoch of $z_\star \sim 1.2$, but the typical low σ galaxy has a much higher M/L (see Figure 6). In the context of our model presented in the previous section where $t_\star \propto (\sigma)^\alpha$, the results of T05 prefer an $\alpha \sim 0.4$–0.45 as opposed to our $\alpha \sim 0.2$. There are two possible explanations for why our results differ from T05. First, the selection limits of T05 z band filter galaxy selection, as opposed to our redder J, biased the resulting sample toward bluer galaxies than our sample,. The second possibility is that the results of T05 are different for lower mass field galaxies because lower mass field galaxies have a different star formation history as compared with lower mass cluster galaxies. Patel et al. (2009b) and Patel et al. (2009a) do find that field and cluster galaxies have different star formation rates and color distributions at $z = 0.83$, possibly explaining the difference between our results and T05.

T05 explain the apparently young stellar populations seen in lower mass galaxies because of small recent episodes of star formation and not because the galaxy population is, as a whole, young, akin to the model of Trager & Somerville (2009). This picture is given more support when compared with the recent results of Thomas et al. (2010), which find that a small fraction of galaxies in the local universe with an E and S0 morphology appear to have had recent, small episodes of star formation. Labeling these young galaxies as "rejuvenated," Thomas et al. (2010) found the fraction of these galaxies increases at lower velocity dispersions, mimicking the steep age–dispersion relation found in T05 and in other work. Rogers et al. (2010) also found a higher fraction of galaxies with recent star formation in lower mass dark matter halos. All of this is consistent with the Trager & Somerville (2009) picture. To explain the results of, say, Cooper et al. (2009) or Rogers et al. (2010), these events would be more common in field-like environments. These are likely the handful of galaxies we observe with bluer colors and lower M/L_B values at lower values of σ. This picture provides a natural explanation for the buildup of the red sequence from $z \sim 1$ until today, see, for example, Harker et al. (2006) or Ruhland et al. (2009), and could provide the progenitors for the apparently young Coma galaxies in Trager et al. (2008).

6. SUMMARY

We have compiled a sample of velocity dispersion measurements of cluster galaxies spanning a broad range in mass at $z = 0.831$. Our sample goes much farther down the mass function than many previous cluster and field samples. Our sample was selected only by J magnitude, effectively in rest-frame r at this redshift, closely mimicking the selection used for many low-redshift samples. No morphological or color information were used in the selection. With *HST*/ACS imaging in the bandpass closest to the rest-frame B, we determined the size and surface brightnesses of the galaxies in our sample. We found that our success at measuring velocity dispersions depended mostly on the magnitude of the galaxies, with no apparent bias in size or surface brightness. We did find that, for the early-type spirals in our sample, we are less likely to measure the dispersions of galaxies with bluer colors, so we proceeded by giving those galaxies higher weight in our analysis.

We determined from our sample the best-fitting FP $\log r_e = a \log \sigma + b \log \langle I_e \rangle + c$, and measure the color and M/L evolution of the early-type population of sub-$L^\star$ galaxies. From our analysis, we conclude the following.

1. We find no evidence that the slope of the FP evolves between Coma and the $z = 0.83$ cluster MS 1054-03. Our sample containing galaxies with $\sigma \sim 160$ km s^{-1} have an FP with the same slope as is found at $z = 0$.
2. The evolution in M/L is observed to be similar to that seen by some previous authors (W04; Holden et al. 2005; vv07), where the M/L of the cluster population evolves with $\Delta \log_{10} M/L_B = -0.50 \pm 0.03$ from $z = 0.023$ and $z = 0.83$, or $d \log_{10} M/L_B = -0.60 \pm 0.04\, dz$, with only a mild σ dependence on the amount of M/L evolution. This in marked contrast to more rapid evolution in field studies, such as T05 or vdW05, or some other cluster results such as Jørgensen et al. (2006).
3. Using the evolution in the M/L_B and in the colors of the galaxies, we find a formation epoch of $z_\star = 1.8^{+0.2}_{-0.2}$ to $z_\star = 2.5^{+0.3}_{-0.2}$, the range depending on the stellar population assumptions we make. This is similar to previous measurements, see, for example, Kelson et al. (2000c), Wuyts et al. (2004), Holden et al. (2005b), and vv07 and is in good agreement with color estimates such as B06 and Mei et al. (2009).
4. The lack of evolution in the tilt of the FP and in the color–σ relations implies little trend in the formation epoch of cluster galaxies with σ. We find $z_\star = 2.3^{+1.3}_{-0.3}$ for the most massive, >300 km s^{-1}, cluster galaxies, while we find $z_\star = 1.7^{+0.3}_{-0.2}$ for those with ~ 160 km s^{-1}. This same lack of evolution in the tilt of the FP and color–σ relation also implies a similar IMF for the lower mass cluster galaxies as is seen at higher masses, with a upper limit of $\Delta x \sim 0.4$ over the mass range we cover, where x is the slope of the IMF.

APPENDIX A

MS 1054-03 SAMPLE

A.1. Fitting Surface Brightness Profiles

For each galaxy, we fit the surface brightness profiles in multiple steps. A Sérsic model was fit first, using values from a catalog derived by SExtractor as initial guesses but with a restriction on n of $1 \leqslant n \leqslant 4$. The output of the Sérsic model was used an initial guess for the de Vaucouleur's model fit, and the Sérsic model was refit using the previous iteration as an initial guess. If the best-fitting Sérsic index is $n = 1$, we refit freezing $n = 1$. This was done to ensure convergence.

Galaxies in crowded environment, generally those near the center of the cluster, were fit simultaneously along with all of

Table A1
Data for Galaxies in MS1054-03

ID	z	$\log_{10}\sigma$ ($\log_{10}$ km s^{-1})	$\log_{10} r_e$[a] ($\log_{10}$ kpc)	q[a]	n[a]	$-0.4\mu_B$[a] (-0.4 mag)	B_z (mag)	$(U-V)_z$[b] (mag)	r_z (mag)	T	J (mag)	$I-J$ (mag)
3500	0.836	$\cdots$	0.679 ± 0.017	0.80	1.6	-9.04	22.85	0.04	22.35	6	20.75	0.52
3533	0.837	2.294 ± 0.028	0.630 ± 0.009	0.84	4.0	-8.59	21.97	1.24	21.24	-5	19.56	1.15
4336	0.835	2.227 ± 0.044	0.200 ± 0.042	0.64	3.5	-8.48	23.85	1.14	23.25	-2	21.61	0.89
4685	0.835	$\cdots$	0.478 ± 0.015	0.47	1.0	-8.91	23.53	0.38	23.07	3	21.48	0.46
4846	0.697	$\cdots$	0.492 ± 0.036	0.90	3.7	-8.73	23.02	0.35	21.71	-5	20.05	1.01
4928	0.851	$\cdots$	0.542 ± 0.015	0.40	1.0	-8.96	23.35	0.50	22.31	4	20.64	1.09
5108	0.840	2.208 ± 0.030	0.287 ± 0.010	0.71	4.0	-8.29	22.95	1.24	22.19	-2	20.52	1.13
5152	0.837	$\cdots$	0.165 ± 0.016	0.92	4.0	-8.17	23.26	1.11	22.79	-5	21.15	0.85
5234	0.837	1.938 ± 0.066	0.046 ± 0.012	0.93	4.0	-8.02	23.48	1.23	22.63	-5	20.98	0.97
5588	0.824	$\cdots$	0.569 ± 0.007	0.92	1.0	-8.79	22.77	0.37	22.18	4	20.52	1.04
5795	0.842	2.245 ± 0.031	0.474 ± 0.009	0.75	4.0	-8.50	22.52	1.22	21.42	-2	19.73	1.25
5894	0.827	$\cdots$	0.297 ± 0.023	0.39	1.0	-8.79	24.13	1.35	1.64	1	0.10	0.00
5987	0.829	2.062 ± 0.046	0.526 ± 0.004	0.79	1.0	-8.78	22.97	0.23	22.53	6	20.91	0.65
6169	0.777	1.946 ± 0.072	0.028 ± 0.016	0.81	2.7	-8.05	23.63	1.40	22.68	-5	21.01	1.12
6191	0.824	2.356 ± 0.028	-0.004 ± 0.013	0.45	4.2	-7.66	22.82	1.27	22.10	-1	20.43	1.07
6333	0.837	2.212 ± 0.028	0.264 ± 0.013	0.41	2.0	-8.36	23.23	1.31	22.62	-2	20.93	1.24
6410	0.833	2.305 ± 0.030	-0.004 ± 0.013	0.49	3.6	-7.92	23.47	1.20	22.92	-2	21.25	1.14
6426	0.832	$\cdots$	0.097 ± 0.021	0.72	3.0	-8.38	24.11	1.22	23.19	-2	21.50	1.27
6448	0.849	2.111 ± 0.063	0.456 ± 0.007	0.54	1.4	-8.58	22.81	0.73	22.52	1	20.91	0.64
6594	0.832	2.264 ± 0.029	0.426 ± 0.016	0.72	3.9	-8.35	22.39	1.21	21.66	-4	19.98	1.16
6630	0.842	$\cdots$	-0.004 ± 0.010	0.60	1.0	-8.15	24.04	0.63	23.04	0	21.39	0.94
6842	0.830	2.010 ± 0.041	0.293 ± 0.020	0.71	3.9	-8.43	23.26	1.04	22.86	-4	21.21	0.96
7075	0.831	2.130 ± 0.087	0.040 ± 0.018	0.79	2.5	-8.22	24.01	1.16	23.43	-9	21.76	1.11
7083	0.835	2.167 ± 0.055	0.275 ± 0.012	0.77	2.6	-8.39	23.25	1.30	21.58	-4	19.88	1.40
7088	0.834	$\cdots$	0.218 ± 0.014	0.80	4.0	-8.49	23.77	1.29	22.48	-5	20.79	1.31
7247	0.821	2.193 ± 0.030	0.680 ± 0.030	0.48	3.5	-8.97	22.66	1.00	22.25	-1	20.59	1.02
7415	0.831	2.309 ± 0.028	0.264 ± 0.009	0.52	2.1	-8.15	22.71	1.23	21.67	-2	20.00	1.19
7534	0.839	2.257 ± 0.041	0.337 ± 0.008	0.45	1.0	-8.51	23.24	0.50	22.28	4	20.62	1.01
7613	0.830	2.103 ± 0.041	0.628 ± 0.003	0.70	1.0	-8.83	22.59	0.53	22.25	8	20.62	0.72
7648	0.833	2.248 ± 0.032	0.043 ± 0.018	0.24	1.7	-8.02	23.48	1.31	22.43	-1	20.74	1.26
7778	0.826	2.211 ± 0.028	0.363 ± 0.013	0.48	2.1	-8.54	23.18	1.10	22.11	-1	20.45	1.04
7937	0.848	2.172 ± 0.033	0.046 ± 0.018	0.28	2.4	-7.91	23.19	1.15	22.30	1	20.62	1.20
8438	0.831	2.210 ± 0.033	0.366 ± 0.016	0.34	2.6	-8.23	22.40	1.12	21.67	1	20.01	1.11
8572	0.825	2.162 ± 0.027	0.099 ± 0.005	0.82	4.0	-7.82	22.70	1.07	22.03	-5	20.37	0.99
8740	0.825	2.487 ± 0.025	0.316 ± 0.014	0.48	3.4	-8.11	22.33	1.45	21.18	-1	19.50	1.20
8771	0.831	2.088 ± 0.052	0.509 ± 0.010	0.75	4.0	-8.45	22.22	0.79	21.67	1	20.01	0.96
8801	0.827	2.226 ± 0.027	0.568 ± 0.007	0.84	4.0	-8.64	22.40	0.47	21.60	-2	19.92	1.16
8839	0.841	$\cdots$	0.298 ± 0.010	0.68	1.4	-8.48	23.36	0.12	22.84	8	21.24	0.58
9061	0.838	2.174 ± 0.029	0.174 ± 0.007	0.80	4.0	-8.05	22.90	1.27	22.12	-4	20.43	1.31
9145	0.835	2.172 ± 0.111	0.489 ± 0.012	0.85	4.0	-8.56	22.59	1.28	21.53	-5	19.88	1.01
9288	0.836	2.127 ± 0.034	0.542 ± 0.012	0.89	2.0	-8.61	22.47	0.74	21.70	4	20.04	1.03
9306	0.829	2.358 ± 0.027	0.464 ± 0.010	0.75	4.0	-8.42	22.38	1.40	21.42	-4	19.75	1.08
10126	0.833	$\cdots$	0.383 ± 0.005	0.93	1.0	-8.52	23.03	-0.04	22.83	8	21.24	0.46
10441	0.829	2.193 ± 0.036	0.394 ± 0.011	0.37	1.0	-8.57	23.10	1.25	22.20	1	20.50	1.29
10480	0.660	$\cdots$	0.337 ± 0.043	0.37	1.3	-8.97	24.38	0.03	23.21	1	21.61	0.55
10806	0.827	$\cdots$	0.673 ± 0.012	0.82	2.1	-8.75	22.15	0.37	21.79	4	20.16	0.78
10829	0.857	$\cdots$	0.633 ± 0.013	0.64	1.0	-9.09	23.22	0.38	22.55	6	20.91	0.85
11217	0.828	2.256 ± 0.035	0.002 ± 0.013	0.64	2.1	-8.06	23.80	1.01	22.99	-5	21.33	1.03
11236	0.828	$\cdots$	0.524 ± 0.016	0.30	1.0	-8.86	23.19	0.49	22.69	3	21.09	0.53
11297	0.836	2.128 ± 0.027	0.249 ± 0.013	0.92	2.9	-8.13	22.73	1.27	22.04	-2	20.39	0.97
11461	0.822	$\cdots$	0.638 ± 0.011	0.61	3.6	-8.32	21.26	0.94	20.63	4	18.98	0.96
11558	0.830	2.192 ± 0.029	0.855 ± 0.034	0.42	4.0	-9.02	21.93	1.03	21.07	4	19.38	1.36
11870	0.827	$\cdots$	0.334 ± 0.023	0.47	1.1	-8.81	24.00	0.47	22.99	0	21.33	1.03
11918	0.833	$\cdots$	-0.319 ± 0.021	0.75	4.0	-6.91	22.52	-0.35	21.76	1	20.14	0.68
11945	0.838	2.329 ± 0.030	0.210 ± 0.008	0.56	4.0	-8.07	22.78	1.09	22.07	-1	20.39	1.22
w1192	0.840	2.156 ± 0.026	0.395 ± 0.005	0.75	4.0	-8.05	21.80	1.34	20.70	-4	19.02	1.15
w1649	$\cdots$	2.386 ± 0.050	0.541 ± 0.006	0.78	4.0	-8.31	21.72	1.34	20.94	-4	19.26	1.24
w2409	$\cdots$	2.458 ± 0.050	0.408 ± 0.009	0.68	3.2	-8.29	22.34	1.43	21.56	-4	19.87	1.26
w3058	0.832	2.496 ± 0.028	1.207 ± 0.010	0.72	3.7	-9.15	20.48	1.31	19.96	-5	18.27	1.28
w3768	$\cdots$	2.346 ± 0.047	0.427 ± 0.004	0.90	4.0	-8.21	22.04	1.26	21.43	-5	19.74	1.30
w3910	$\cdots$	2.470 ± 0.062	0.163 ± 0.007	0.42	4.0	-7.73	22.15	1.49	21.58	-2	19.91	1.18
w4345	$\cdots$	2.526 ± 0.044	0.546 ± 0.009	0.68	3.4	-8.28	21.62	1.38	20.74	-5	19.05	1.28
w4520	$\cdots$	2.508 ± 0.040	1.339 ± 0.013	0.64	4.9	-9.22	20.00	1.40	19.72	-5	18.03	1.34
w4705	$\cdots$	2.403 ± 0.062	0.455 ± 0.007	0.28	1.6	-8.29	22.11	0.73	21.15	-1	19.51	0.89
w4926	$\cdots$	2.491 ± 0.053	0.267 ± 0.007	0.46	4.0	-8.00	22.32	1.42	21.48	-3	19.78	1.35

Table A1
(Continued)

ID	z	$\log_{10}\sigma$ ($\log_{10}$ km s^{-1})	$\log_{10} r_e$[a] ($\log_{10}$ kpc)	q[a]	n[a]	$-0.4\mu_B$[a] (-0.4 mag)	B_z (mag)	$(U-V)_z$[b] (mag)	r_z (mag)	T	J (mag)	$I-J$ (mag)
w5280	$\cdots$	2.413 ± 0.052	0.335 ± 0.011	0.36	2.3	-8.14	22.31	1.34	21.42	-2	19.73	1.23
w5298	$\cdots$	2.453 ± 0.060	0.331 ± 0.012	0.51	2.5	-8.24	22.60	1.22	21.76	-2	20.08	1.19
w5347	$\cdots$	2.405 ± 0.041	0.234 ± 0.008	0.41	2.3	-7.78	21.93	1.10	20.66	-1	19.00	1.08
w5450	$\cdots$	2.369 ± 0.048	0.904 ± 0.005	0.79	4.0	-8.78	21.09	1.25	20.29	-5	18.60	1.29
w5529	$\cdots$	2.260 ± 0.055	0.349 ± 0.009	0.70	2.8	-8.14	22.25	1.27	21.40	-5	19.72	1.22
w5577	$\cdots$	2.484 ± 0.057	0.320 ± 0.016	0.49	3.2	-8.07	22.21	1.28	21.59	-4	19.90	1.26
w5666	$\cdots$	2.456 ± 0.035	0.685 ± 0.005	0.67	4.0	-8.45	21.34	1.29	20.74	-1	19.06	1.18
w5756	0.831	2.379 ± 0.026	0.577 ± 0.004	0.98	4.0	-8.43	21.83	1.30	21.28	-5	19.59	1.29
w5840	$\cdots$	2.405 ± 0.038	0.181 ± 0.007	0.60	4.0	-7.97	22.66	1.17	21.04	-5	19.36	1.17
w6036	$\cdots$	2.396 ± 0.042	0.478 ± 0.012	0.82	3.6	-8.30	22.01	1.38	21.22	-1	19.52	1.35
w6301	$\cdots$	2.438 ± 0.059	0.438 ± 0.004	0.80	4.0	-8.18	21.91	1.31	21.19	-5	19.50	1.23

Notes.
[a] These are the measured values from fitting a elliptical Sérsic model to the two-dimensional images.
[b] $U - V_z$ refers to the $U - V$ color as if measured by U and V filters redshifted to $z = 0.831$, the redshift of the cluster.
[c] T refers to the morphological class. The scheme is the same as Postman et al. (2005). E: $-5 \leqslant T \leqslant -3$, S0: $-2 \leqslant T \leqslant -1$, with spirals $0 \leqslant T \leqslant 10$.
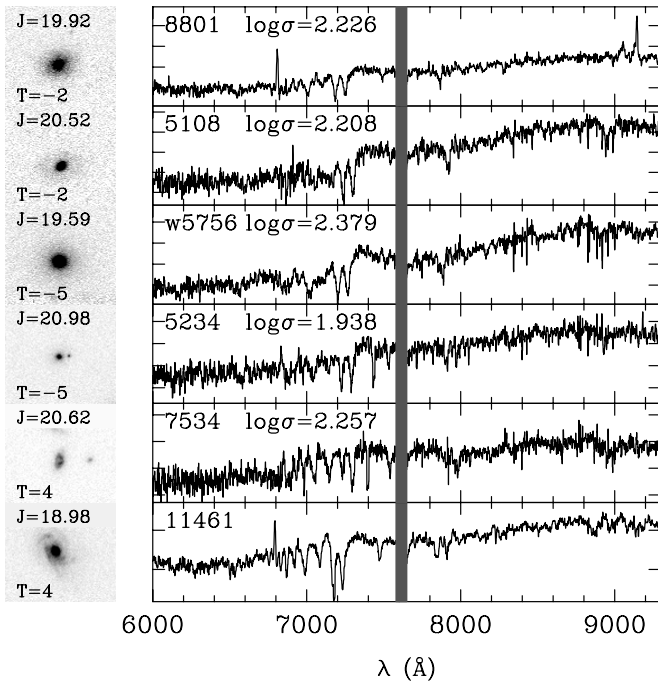

Figure A1. Example spectra and images. All images are $5\farcs0$ on a side and all spectra are in the observed frame. The vertical gray band masks the atmospheric absorption from the A band. The top three galaxies represent typical objects in our sample, $19.5 < J < 20.5$ with E and S0 morphologies and $\log\sigma > 2.2$. The brightest of these galaxies, w5756, is one of the three galaxies from W04 which we re-observed. 5234 is the faintest galaxy for which we measured a σ value. The bottom two galaxies are both late-type systems, with the stretch for 7534 adjusted to illustrate this. 7534 has strong enough metal absorption lines for us to measure a dispersion. In 11461, the strong Balmer absorption and lack of metal lines prevented us from measuring a σ, despite its bright J magnitude. Both 5234 and 11461 were imaged using the I_{814} on ACS while the remaining galaxies were observed with i_{775} filter.

those galaxies' neighbors. We use the sizes from the SExtractor catalog to find galaxies with close neighbors. All galaxies within a radius twice the size of a target galaxy were fit along with the target galaxy. In addition, galaxies outside of that radius but with sizes such that the target galaxy lies within twice their size were also included in the joint fit. This later criterion was chosen because particularly large galaxies, like the brightest galaxy

of the cluster, often have extended surface brightness profiles. After the fitting process, if the radii of the target galaxy were significantly larger than the initial SExtractor guess, we refit including more neighboring galaxies. In all cases, neighboring galaxies were fit with a Sérsic model constrained to lie in $1 \leqslant n \leqslant 4$.

We note here that the ACS magnitudes and surface brightnesses have been adjusted by the offsets as we computed from simulations that are listed in Section 2.2.

A.2. Errors on the Morphologies

A number of galaxies in our sample were morphologically typed multiple times. All of the galaxies in our sample were classified by Marc Postman twice, once for Postman et al. (2005) and once for the parent sample that the galaxies in this paper are drawn from. In addition, many of these galaxies were classified in WFPC2 imaging (Tran et al. 2007). For the purposes of this paper, the main classification is the distinction between a late-type or an early-type system, where the former are spiral and irregular galaxies while the later are ellipticals and S0 galaxies. The comparison in Postman et al. (2005) finds that 10% of the galaxies in the ACS sample are identified as spirals in the WFPC2 or vice versa. When comparing that two separate classifications done by Marc Postman, we find that 92% of galaxies are grouped in the same two broad bins.

A.3. Summary of the Data

We list all of the galaxies targeted in Table A1. For each galaxy, we list the redshift and dispersion, if available. For a summary of why some galaxies do not have dispersions, see Section 2.3.2. The galaxies in the sample of W04 are listed with a "w" in front of the identification number. The galaxies with redshifts are those we re-observed as part of our program. All of the other galaxies have spectroscopic information from W04 which does not list redshifts, though those can be found in Tran et al. (2007).

APPENDIX B

COMA DATA

Here, we list the compilation of Coma data (Table A2). These are galaxies in the JFK96 catalog with the corresponding

Table A2
Data for Galaxies in Coma

ID	$\log_{10}\sigma$ ($\log_{10}$ km s^{-1})	$\log_{10} r_e$ ($\log_{10}$ kpc)	q	n	$-0.4\mu_B$ (-0.4 mag)	B_z (mag)	$(U-V)_z$ (mag)
024	2.366	0.290	0.41	4.0	-8.59	15.03	$\cdots$
027	2.015	0.228	0.70	2.9	-8.87	16.05	$\cdots$
031	2.416	1.230	0.58	4.0	-9.57	12.79	$\cdots$
046	2.383	0.519	0.68	4.0	-8.78	14.36	$\cdots$
049	2.418	0.757	0.54	4.0	-8.97	13.66	$\cdots$
057	2.232	0.431	0.65	3.4	-8.71	14.63	$\cdots$
058	2.263	0.805	0.77	4.0	-9.40	14.50	$\cdots$
065	2.091	0.364	0.78	2.8	-9.02	15.74	1.48
067	2.215	0.014	0.91	3.2	-8.44	16.04	1.44
068	2.138	0.564	0.95	4.0	-9.19	15.17	1.46
069	2.299	0.450	0.82	3.9	-8.85	14.89	1.60
070	2.199	0.313	0.96	4.0	-8.78	15.40	1.48
072	2.165	0.179	0.48	2.9	-8.55	15.50	1.39
078	2.293	0.645	0.83	4.0	-9.01	14.31	$\cdots$
081	2.183	0.456	0.72	4.0	-9.16	15.64	$\cdots$
087	1.925	0.065	0.84	3.2	-8.76	16.59	1.28
088	2.443	0.093	0.56	4.0	-8.36	15.44	1.56
098	2.200	0.332	0.88	3.6	-8.79	15.33	$\cdots$
101	2.140	0.162	0.57	3.5	-8.64	15.81	1.43
103	2.356	0.349	0.53	4.0	-8.66	14.92	1.50
104	2.301	0.195	0.37	3.6	-8.58	15.50	1.51
105	2.323	0.600	0.69	3.8	-8.95	14.40	1.58
106	2.247	0.063	0.89	3.5	-8.56	16.10	1.32
107	1.852	0.256	0.82	2.1	-8.93	16.06	1.30
109	2.276	0.329	0.95	3.9	-8.80	15.38	1.58
116	2.143	0.593	0.49	4.0	-9.33	15.38	1.46
118	2.237	0.478	0.87	3.5	-8.92	14.92	1.51
119	2.223	0.246	0.56	4.0	-8.85	15.90	1.37
120	2.164	0.387	0.82	3.4	-8.62	14.62	1.46
121	2.340	0.077	0.70	2.2	-8.54	15.97	1.47
122	1.992	0.556	0.86	4.0	-9.21	15.26	1.29
124	2.277	0.272	0.47	2.7	-8.62	15.19	1.48
125	2.267	-0.061	0.70	4.0	-8.33	16.14	1.35
128	2.065	0.434	0.93	4.0	-9.17	15.76	1.27
129	2.376	1.644	0.74	4.0	-10.01	11.81	1.71
130	2.352	0.489	0.58	4.0	-8.88	14.78	1.50
131	2.251	0.789	0.56	4.0	-9.33	14.38	1.57
132	2.142	0.505	0.85	4.0	-9.36	15.89	1.42
133	2.375	0.264	0.62	4.0	-8.55	15.08	1.46
135	1.920	0.140	0.38	3.1	-8.92	16.62	1.40
136	2.221	-0.172	0.80	2.5	-8.19	16.34	1.37
137	2.245	0.364	0.62	3.6	-8.71	14.96	$\cdots$
143	2.344	0.826	0.73	3.3	-9.25	14.00	1.68
144	2.238	0.596	0.49	4.0	-9.07	14.70	1.48
145	2.152	0.415	0.39	3.3	-9.01	15.47	1.48
146	2.042	0.549	0.63	3.2	-9.24	15.37	1.37
148	2.572	1.234	0.39	4.0	-9.33	12.18	1.75
150	2.044	0.353	0.42	4.0	-8.94	15.61	1.40
151	2.184	0.784	0.66	4.0	-9.32	14.39	1.42
152	2.217	0.616	0.63	4.0	-9.27	15.10	1.52
153	2.153	0.359	0.89	4.0	-8.97	15.65	1.44
155	2.203	0.783	0.74	4.0	-9.35	14.48	1.50
156	2.025	0.268	0.59	3.6	-9.08	16.36	1.29
157	2.142	0.305	0.54	4.0	-8.97	15.92	1.32
159	2.306	0.556	0.37	3.4	-8.88	14.43	1.54
160	2.284	0.513	0.68	3.9	-9.04	15.05	1.50
161	2.251	0.547	0.53	4.0	-8.95	14.65	$\cdots$
167	2.336	0.509	0.74	3.9	-8.81	14.49	1.53
168	2.347	0.264	0.93	2.5	-8.48	14.88	1.53
170	2.174	0.445	0.52	3.7	-9.00	15.30	1.44
172	2.227	0.143	0.63	3.6	-8.52	15.60	1.45
173	2.179	0.161	0.88	4.0	-8.66	15.87	1.41
174	2.287	0.014	0.24	2.3	-8.28	15.64	1.50
175	2.263	0.378	0.62	2.9	-8.78	15.08	1.58
176	2.249	0.146	0.87	1.6	-8.60	15.78	1.50

Table A2
(Continued)

ID	$\log_{10}\sigma$ ($\log_{10}$ km s^{-1})	$\log_{10} r_e$ ($\log_{10}$ kpc)	q	n	$-0.4\mu_B$ (-0.4 mag)	B_z (mag)	$(U-V)_z$ (mag)
177	2.038	0.218	0.18	3.7	-8.93	16.25	1.40
179	2.404	0.478	0.74	4.0	-8.63	14.20	1.51
181	2.194	0.089	0.96	3.9	-8.60	16.07	1.38
191	1.994	0.007	0.87	2.3	-8.54	16.32	$\cdots$
192	1.989	0.178	0.23	1.6	-8.65	15.75	$\cdots$
193	2.101	0.155	0.38	2.9	-8.74	16.08	$\cdots$
194	2.398	0.646	0.68	4.0	-8.93	14.10	$\cdots$
204	2.116	0.416	0.31	4.0	-9.06	15.57	$\cdots$
206	2.351	0.627	0.28	3.3	-8.83	13.96	$\cdots$
207	2.192	0.181	0.24	2.6	-8.67	15.79	$\cdots$
210	2.246	0.153	0.51	3.4	-8.53	15.58	$\cdots$
217	2.317	0.766	0.81	4.0	-9.18	14.12	$\cdots$
238	2.041	0.037	0.86	3.4	-8.51	16.10	$\cdots$
239	2.359	0.791	0.62	4.0	-9.18	14.01	$\cdots$
240	2.415	1.024	0.61	4.0	-9.31	13.18	$\cdots$

selection of E and S0 galaxies above a r magnitude limit of $r < 15.1$ mag AB. Each galaxy has a surface brightness profile derived from reprocessed SDSS imaging, see Holden et al. (2007). This processing mimics what was done for MS 1054-03, so we have comparable data sets.

As discussed in Holden et al. (2007), each galaxy has a B_z magnitude derived from the observed g and $g - r$. Our B values match the values from JFK96 and we find good agreement between our $B - V$ colors derived from the $g - r$ imaging and those of Eisenhardt et al. (2007).

The SDSS u imaging is, however, shallow, in comparison to that of Eisenhardt et al. (2007). Therefore, we use the colors from that paper. The colors we list below are extinction corrected and in the redshifted $(U - V)_z$ filters. We start with the colors from Table 8 of Eisenhardt et al. (2007). We use the extinction corrections from Schlegel et al. (1998), namely, $A_U = 0.052$ and $A_V = 0.032$. We redshift the $U - V$ color with the relation $(U - V)_z = (U - V) - 0.067(U - V)^2 + 0.220(U - V) - 0.220$ as noted in Section 2.4.

All dispersions come from JFK96. These were measured in equivalent manner as the ones at $z = 0.83$.

REFERENCES

Auger, M. W., Treu, T., Gavazzi, R., Bolton, A. S., Koopmans, L. V. E., & Marshall, P. J. 2010, ApJ, 721, L163
Bell, E. F., et al. 2004, ApJ, 608, 752
Bernardi, M., Nichol, R. C., Sheth, R. K., Miller, C. J., & Brinkmann, J. 2006, AJ, 131, 1288
Bernardi, M., et al. 2003a, AJ, 125, 1866
Bernardi, M., et al. 2003b, AJ, 125, 1882
Berrier, J. C., Stewart, K. R., Bullock, J. S., Purcell, C. W., Barton, E. J., & Wechsler, R. H. 2009, ApJ, 690, 1292
Blain, A. W., Jameson, A., Smail, I., Longair, M. S., Kneib, J., & Ivison, R. J. 1999, MNRAS, 309, 715
Blakeslee, J. P., et al. 2006, ApJ, 644, 30
Bower, R. G., Lucey, J. R., & Ellis, R. S. 1992, MNRAS, 254, 601
Brammer, G. B., & van Dokkum, P. G. 2007, ApJ, 654, L107
Brammer, G. B., et al. 2009, ApJ, 706, L173
Bruzual, G., & Charlot, S. 2003, MNRAS, 344, 1000
Buser, R. 1978, A&A, 62, 411
Coleman, G. D., Wu, C.-C., & Weedman, D. W. 1980, ApJS, 43, 393
Cooper, M. C., Gallazzi, A., Newman, J. A., & Yan, R. 2009, MNRAS, 402, 1942
Dickinson, M., Papovich, C., Ferguson, H. C., & Budavári, T. 2003, ApJ, 587, 25
Djorgovski, S., & Davis, M. 1987, ApJ, 313, 59

Eisenhardt, P., De Propris, R., Gonzalez, A. H., Stanford, S. A., & Dickinson, M. E. 2007, ApJS, 169, 225

Eisenhardt, P. R. M., et al. 2008, ApJ, 684, 905

Faber, S. M., Dressler, A., Davies, R. L., Burstein, D., & Lynden-Bell, D. 1987, in Nearly Normal Galaxies, From the Planck Time to the Present, ed. S. M. Faber (New York: Springer-Verlag), 175

Gallazzi, A., Charlot, S., Brinchmann, J., & White, S. D. M. 2006, MNRAS, 370, 1106

Gebhardt, K., et al. 2003, ApJ, 597, 239

Graves, G. J., Faber, S. M., & Schiavon, R. P. 2009a, ApJ, 693, 486

Graves, G. J., Faber, S. M., & Schiavon, R. P. 2009b, ApJ, 698, 1590

Harker, J. J., Schiavon, R. P., Weiner, B. J., & Faber, S. M. 2006, ApJ, 647, L103

Holden, B. P., Stanford, S. A., Eisenhardt, P. R., & Dickinson, M. 2004, AJ, 127, 2484

Holden, B. P., et al. 2005a, ApJ, 626, 809

Holden, B. P., et al. 2005b, ApJ, 620, L83

Holden, B. P., et al. 2006, ApJ, 642, L123

Holden, B. P., et al. 2007, ApJ, 670, 190

Holden, B. P., et al. 2009, ApJ, 693, 617

Horne, K. 1986, PASP, 98, 609

Hyde, J. B., & Bernardi, M. 2009, MNRAS, 396, 1171

Jørgensen, I., Chiboucas, K., Flint, K., Bergmann, M., Barr, J., & Davies, R. 2006, ApJ, 639, L9

Jørgensen, I., Chiboucas, K., Flint, K., Bergmann, M., Barr, J., & Davies, R. 2007, ApJ, 654, L179

Jørgensen, I., Franx, M., & Kjaergaard, P. 1996, MNRAS, 280, 167

Kelson, D. D. 2003, PASP, 115, 688

Kelson, D. D., Illingworth, G. D., Franx, M., & van Dokkum, P. G. 2001, ApJ, 552, L17

Kelson, D. D., Illingworth, G. D., Franx, M., & van Dokkum, P. G. 2006, ApJ, 653, 159

Kelson, D. D., Illingworth, G. D., van Dokkum, P. G., & Franx, M. 2000a, ApJ, 531, 137

Kelson, D. D., Illingworth, G. D., van Dokkum, P. G., & Franx, M. 2000b, ApJ, 531, 159

Kelson, D. D., Illingworth, G. D., van Dokkum, P. G., & Franx, M. 2000c, ApJ, 531, 184

Kelson, D. D., van Dokkum, P. G., Franx, M., Illingworth, G. D., & Fabricant, D. 1997, ApJ, 478, L13

Kriek, M., van der Wel, A., van Dokkum, P. G., Franx, M., & Illingworth, G. D. 2008, ApJ, 682, 896

La Barbera, F., de Carvalho, R. R., de La Rosa, I. G., & Lopes, P. A. A. 2010a, MNRAS, in press (arXiv:0912.4558)

La Barbera, F., Lopes, P. A. A., de Carvalho, R. R., de La Rosa, I. G., & Berlind, A. A. 2010b, MNRAS, in press (arXiv:1003.1119)

Madau, P., Pozzetti, L., & Dickinson, M. 1998, ApJ, 498, 106

Mancone, C. L., Gonzalez, A. H., Brodwin, M., Stanford, S. A., Eisenhardt, P. R. M., Stern, D., & Jones, C. 2010, ApJ, 720, 284

Maraston, C. 2005, MNRAS, 362, 799

Mei, S., et al. 2009, ApJ, 690, 42

Nelan, J. E., Smith, R. J., Hudson, M. J., Wegner, G. A., Lucey, J. R., Moore, S. A. W., Quinney, S. J., & Suntzeff, N. B. 2005, ApJ, 632, 137

Oke, J. B., et al. 1995, PASP, 107, 375

Patel, S. G., Holden, B. P., Kelson, D. D., Illingworth, G. D., & Franx, M. 2009a, ApJ, 705, L67

Patel, S. G., Kelson, D. D., Holden, B. P., Illingworth, G. D., Franx, M., van der Wel, A., & Ford, H. 2009b, ApJ, 694, 1349

Peng, C. Y., Ho, L. C., Impey, C. D., & Rix, H.-W. 2002, AJ, 124, 266

Postman, M., et al. 2005, ApJ, 623, 721

Renzini, A. 2006, ARA&A, 44, 141

Rogers, B., Ferreras, I., Pasquali, A., Bernardi, M., Lahav, O., & Kaviraj, S. 2010, MNRAS, 405, 329

Rudnick, G., et al. 2003, ApJ, 599, 847

Ruhland, C., Bell, E. F., Häußler, B., Taylor, E. N., Barden, M., & McIntosh, D. H. 2009, ApJ, 695, 1058

Saglia, R. P., et al. 2010, A&A, in press (arXiv:1009.0645)

Salpeter, E. E. 1955, ApJ, 121, 161

Schlegel, D. J., Finkbeiner, D. P., & Davis, M. 1998, ApJ, 500, 525

Smith, R. J., Lucey, J. R., Hudson, M. J., & Bridges, T. J. 2009, MNRAS, 398, 119

Stanford, S. A., Eisenhardt, P. R., & Dickinson, M. 1998, ApJ, 492, 461

Steidel, C. C., Adelberger, K. L., Giavalisco, M., Dickinson, M., & Pettini, M. 1999, ApJ, 519, 1

Thomas, D., Maraston, C., Schawinski, K., Sarzi, M., & Silk, J. 2010, MNRAS, 404, 1775

Tinsley, B. M. 1972, ApJ, 178, 319

Tortora, C., Napolitano, N. R., Romanowsky, A. J., Capaccioli, M., & Covone, G. 2009, MNRAS, 396, 1132

Trager, S. C., Faber, S. M., & Dressler, A. 2008, MNRAS, 386, 715

Trager, S. C., Faber, S. M., Worthey, G., & González, J. J. 2000a, AJ, 120, 165

Trager, S. C., Faber, S. M., Worthey, G., & González, J. J. 2000b, AJ, 119, 1645

Trager, S. C., & Somerville, R. S. 2009, MNRAS, 395, 608

Tran, K.-V. H., Franx, M., Illingworth, G. D., van Dokkum, P., Kelson, D. D., Blakeslee, J. P., & Postman, M. 2007, ApJ, 661, 750

Treu, T., Auger, M. W., Koopmans, L. V. E., Gavazzi, R., Marshall, P. J., & Bolton, A. S. 2010, ApJ, 709, 1195

Treu, T., Ellis, R. S., Liao, T. X., & van Dokkum, P. G. 2005a, ApJ, 622, L5

Treu, T., et al. 2005b, ApJ, 633, 174

van de Ven, G., van Dokkum, P. G., & Franx, M. 2003, MNRAS, 344, 924

van der Marel, R. P., & van Dokkum, P. G. 2007a, ApJ, 668, 738

van der Marel, R. P., & van Dokkum, P. G. 2007b, ApJ, 668, 756

van der Wel, A., Franx, M., van Dokkum, P. G., & Rix, H.-W. 2004, ApJ, 601, L5

van der Wel, A., Franx, M., van Dokkum, P. G., Rix, H.-W., Illingworth, G. D., & Rosati, P. 2005, ApJ, 631, 145

van der Wel, A., Franx, M., Wuyts, S., van Dokkum, P. G., Huang, J., Rix, H., & Illingworth, G. D. 2006, ApJ, 652, 97

van der Wel, A., Holden, B. P., Zirm, A. W., Franx, M., Rettura, A., Illingworth, G. D., & Ford, H. C. 2008, ApJ, 688, 48

van der Wel, A., & van der Marel, R. P. 2008, ApJ, 684, 260

van Dokkum, P. G. 2008, ApJ, 674, 29

van Dokkum, P. G., & Ellis, R. S. 2003, ApJ, 592, L53

van Dokkum, P. G., & Franx, M. 1996, MNRAS, 281, 985

van Dokkum, P. G., & Franx, M. 2001, ApJ, 553, 90

van Dokkum, P. G., Franx, M., Kelson, D. D., & Illingworth, G. D. 2001, ApJ, 553, L39

van Dokkum, P. G., & Stanford, S. A. 2003, ApJ, 585, 78

van Dokkum, P., & van der Marel, R. 2007, ApJ, 655, 30

Wuyts, S., van Dokkum, P. G., Kelson, D. D., Franx, M., & Illingworth, G. D. 2004, ApJ, 605, 677

Zirm, A. W., et al. 2008, ApJ, 680, 224